Flavor anomalies in supersymmetric scenarios with nonminimal flavor violation

M. A. Boussejra,[1,*] F. Mahmoudi,[1,2,†] and G. Uhlrich[1,3,‡]

[1]*Université de Lyon, Université Claude Bernard Lyon 1, CNRS/IN2P3, Institut de Physique des 2 Infinis de Lyon, UMR 5822, F-69622 Villeurbanne, France*
[2]*Theoretical Physics Department, CERN, CH-1211 Geneva 23, Switzerland*
[3]*Département de physique nucléaire et corpusculaire, Université de Genève, CH-1211 Geneva, Switzerland*

(Received 3 February 2022; accepted 5 July 2022; published 21 July 2022)

Motivated by tensions between experimental measurements and SM predictions in $b \to s\ell^+\ell^-$ transitions, we present the first study of nonminimal flavor-violating minimal supersymmetric Standard Model (MSSM) scenarios contributing to the relevant Wilson coefficients to address the observed anomalies using `SuperIso` and `MARTY`. We calculate the full one-loop analytical contributions of the general MSSM to Wilson coefficients relevant for flavor anomalies, together with the anomalous muon magnetic dipole moment $(g-2)_\mu$. We show that, after imposing theoretical constraints on the flavor-violating parameters, we can find scenarios in agreement with the experimental measurements that can address at the same time the tensions in flavor observables and in $(g-2)_\mu$.

DOI: 10.1103/PhysRevD.106.015018

I. INTRODUCTION

In recent years, impressive progress has been achieved in studying and measuring semileptonic B decays. In particular, neutral currents with $b \to s$ transitions offer a plethora of clean observables that have been under scrutiny, as they present tensions with the Standard Model (SM) predictions. The first tension, at the level of 3σ, was reported in 2013 in the measurement of angular observables related to $B \to K^*\mu^+\mu^-$ decay [1]. Since then, similar tensions have been observed in several decays, such as $B \to K\mu^+\mu^-$, $B_s \to \phi\mu^+\mu^-$, and $\Lambda_b \to \Lambda\mu^+\mu^-$ [2–5]. In addition, LHCb measured lepton-flavor-universality-violating (LFUV) ratios $R_{K^{(*)}} = \mathrm{BR}(B \to K^{(*)}\mu\mu)/\mathrm{BR}(B \to K^{(*)}ee)$, that are predicted very precisely in the SM, and confirmed the tension with the SM with about 3σ significance for low dilepton mass squared (q^2) [6,7]. Interestingly, all these deviations point to a coherent and consistent pattern, and can find a common explanation from new physics (NP) contributing to the Wilson coefficients C_9 (as was shown in, e.g., Refs. [8–11]).

While LFUV observables have theoretical uncertainties at the percent level (or below) due to the cancellation of hadronic uncertainties in the ratios, the rest of the $b \to s$ observables are subject to assumptions made for the nonlocal hadronic effects and generally suffer from larger theoretical uncertainties [12]. In this analysis, we consider the minimal supersymmetric Standard Model (MSSM) [13,14], which predicts a superpartner particle (sparticle) to each SM field, together with an additional Higgs doublet. As supersymmetry (SUSY) is not observed at low energy scales, it needs to be a broken symmetry of nature. To preserve some of the nice features of supersymmetry, it should be "softly" broken, namely by introducing a SUSY-violating effective Lagrangian $\mathcal{L}_{\mathrm{SOFT}}$, that contains all necessary couplings and masses, adding up to 105 new free parameters.

Until very recently, due to obvious computational challenges, the whole MSSM has been little studied. Indeed, more constrained SUSY models were devised to allow for doable calculations and computations, through well-motivated and seemingly reasonable, but not physically founded assumptions. Such models with simplifications at the GUT scale consider a handful of parameters, like the constrained MSSM (cMSSM) [15]. More recently, the phenomenological MSSM (pMSSM), which considers CP conservation and minimal flavor violation (MFV) simplifications [16], entered within computational reach with its 19 free parameters [17–21]. These models fail to provide a SUSY scenario fully compatible with the aforementioned flavor

*boussejra@ipnl.in2p3.fr
†nazila@cern.ch
‡gregoire.uhlrich@unige.ch

anomalies if R-parity is conserved [22] (for R-parity-violating models, see, e.g., Refs. [23,24]).

In this work, following our preliminary results [25], we will go one step further and consider for the first time a more general setup, based on the assumptions of the pMSSM but including in addition nonminimal flavor violation (NMFV) in the squark sector, as a candidate for the explanation of the flavor anomalies in the $b \to sll$ transitions. NMFV allows for sizeable flavor-changing neutral current (FCNC) effects coming directly from the squark mass matrices at the weak scale, whose off-diagonal entries are then considered as new free parameters with respect to MFV scenarios. We will first consider NMFV contributions to Wilson coefficients through the mass insertion approximation (MIA) and show that the new FCNCs can highly affect the value of C_9 in some scenarios, while still being compatible with the rest of the $b \to s$ constraints. Then, we will present the first analytical calculation of the general contributions to C_7, C_9, C_{10}, and also $(g-2)_\mu$ in the full MSSM with 105 parameters, and their evaluation for particular NMFV scenarios with 42 parameters.

The paper is organized as follows: Section II describes the theoretical context of our analysis. In Sec. III, the flavor-violating parameters are introduced in the mass insertion approximation, and their new contributions to Wilson coefficients are defined. In Sec. IV, the numerical setup for our scans is presented. Section V shows and discusses how the NMFV models may fit the flavor anomalies. In Sec. VI, we present the first full analytical evaluation of the Wilson coefficients and $(g-2)_\mu$, using MARTY [26,27], in the MSSM and their evaluation in NMFV scenarios, confronting the results to the expected experimental values. Finally, the conclusions are given in Sec. VII.

II. THEORETICAL CONTEXT

In the MSSM, the most general soft supersymmetry-breaking Lagrangian can be written as: $-\mathcal{L}_{\rm SOFT} = -\mathcal{L}_{\rm gaugino} - \mathcal{L}_{\rm sfermions} - \mathcal{L}_{\rm Higgs} - \mathcal{L}_{\rm tril.}$, where the different terms are [16,28]

(1) Mass terms for the gluinos, winos, and binos:

$$-\mathcal{L}_{\rm gaugino} = \frac{1}{2}\left[M_1 \tilde{B}\,\tilde{B} + M_2 \sum_{a=1}^{3} \tilde{W}^a \tilde{W}_a + M_3 \sum_{a=1}^{8} \tilde{G}^a \tilde{G}_a + \text{H.c.}\right], \tag{2.1}$$

where $\tilde{B}$, $\tilde{W}$, and $\tilde{G}$ are the bino, wino, and gluino fields, respectively.

(2) Mass terms for the scalar fermions:

$$-\mathcal{L}_{\tilde{f}} = \sum_{i,j=\text{gen}} \tilde{Q}_i^\dagger (M_{\tilde{Q}}^2)_{ij} \tilde{Q}_j + \tilde{L}_i^\dagger (M_{\tilde{L}}^2)_{ij} \tilde{L}_j + \tilde{U}_i^\dagger (M_{\tilde{U}}^2)_{ij} \tilde{U}_j + \tilde{D}_i^\dagger (M_{\tilde{D}}^2)_{ij} \tilde{D}_j + \tilde{E}_i^\dagger (M_{\tilde{E}}^2)_{ij} \tilde{E}_j, \tag{2.2}$$

where $\tilde{Q}_i$ and $\tilde{L}_i$ are the left-handed squarks and sleptons, respectively, with their right-handed counterparts $\tilde{U}$, $\tilde{D}$, and $\tilde{E}$ [no right-handed (s)neutrinos are assumed]. The indices i, j run over generation, and all scalar squared mass matrices are Hermitian.

(3) Mass and bilinear terms for the Higgs bosons:

$$-\mathcal{L}_{\rm Higgs} = m_{H_u}^2 H_u^\dagger H_u + m_{H_d}^2 H_d^\dagger H_d + \mu H_u.H_d + \text{H.c.}, \tag{2.3}$$

where μ is the supersymmetric Higgs mass parameter.

(4) Trilinear couplings between sfermions and Higgs bosons:

$$-\mathcal{L}_{\rm tril.} = \sum_{i,j=\text{gen}} A_{ij}^u Y_{ij}^u \tilde{u}_{R_i} H_u.\tilde{Q}_j + A_{ij}^d Y_{ij}^d \tilde{d}_{R_i} H_d.\tilde{Q}_j + A_{ij}^l Y_{ij}^l \tilde{l}_{R_i} H_u.\tilde{L}_j + \text{H.c.}, \tag{2.4}$$

where A_{ij}^f are the general 3×3 complex soft SUSY-breaking scalar trilinear coupling matrices between Higgs fields (H_u,H_d) and sfermions, in generation basis.

Several mixing effects arise in the general MSSM. In particular, the electroweak gauginos mix together with the Higgsinos and give rise to the chargino and neutralino mass eigenstates. The chargino mixing matrix in the weak eigenstate $(\tilde{W}^+, \tilde{H}_u^+, \tilde{W}^-, \tilde{H}_d^-)$ basis is given by

$$M_\chi = \begin{pmatrix} M_2 & \sqrt{2} M_W \sin\beta \\ \sqrt{2} M_W \cos\beta & \mu \end{pmatrix}, \tag{2.5}$$

where μ is the Higgs quadratic coupling and M_2 is the soft SUSY-breaking wino mass. The β parameter is related to the vacuum expectation values of the two Higgs doublets present in the MSSM by

$$\tan\beta \equiv \frac{v_u}{v_d}, \tag{2.6}$$

with $v_u = \langle H_u^0 \rangle = v \sin\beta$, and $v_d = \langle H_d^0 \rangle = v \cos\beta$.

The 2×2 unitary matrices U and V which diagonalize the chargino mass matrix M_χ are defined as

$$U^* M_\chi V^{-1} = \mathrm{diag}(M_{\chi_1^\pm}, M_{\chi_2^\pm}). \tag{2.7}$$

Their explicit expressions can be found in, e.g., Refs. [16,29,30].

In the other sectors, the MFV hypothesis limits the mixing of squarks to the third generation only. This approach is still widely used in the study of the MSSM. If the MFV hypothesis is relaxed for other generations, a rich mixing dynamic arises. Concentrating on the squark sector in such a NMFV model, and starting from the Lagrangian in Eq. (2.2), one can define the super-CKM (sCKM) basis so that it rotates the (s)quarks' superfields in flavor space, making the quark mass matrices $m_{u,d}$ diagonal. This flavor alignment between quarks and squarks does not imply diagonal squark mass matrices, and it can yield substantial flavor-changing effects.

In the same manner as Ref. [29], let

$$\tilde{\boldsymbol{f}} \equiv \begin{pmatrix} \tilde{f}_L \\ \tilde{f}_R \end{pmatrix} \tag{2.8}$$

be a six-component vector, where $\tilde{f}_L, \tilde{f}_R$ are spanning generation space. We can therefore write the 6×6 flavor mixed squared fermion mass matrices as

$$\mathcal{M}^2_{\tilde{f}} = \begin{pmatrix} \mathcal{M}^2_{\tilde{f}_{LL}} & \mathcal{M}^2_{\tilde{f}_{RL}} \\ \mathcal{M}^2_{\tilde{f}_{LR}} & \mathcal{M}^2_{\tilde{f}_{RR}} \end{pmatrix}. \tag{2.9}$$

Collecting all sfermion mass terms in Eq. (2.2) and using Eq. (2.9),

$$-\mathcal{L}_{\mathcal{M}^2_{\tilde{f}}} = \sum_{\tilde{f}} \tilde{\boldsymbol{f}}^\dagger \mathcal{M}^2_{\tilde{f}} \tilde{\boldsymbol{f}}. \tag{2.10}$$

This defines the relevant mass matrices for the squark sector: $\mathcal{M}^2_{\tilde{\boldsymbol{u}}}, \mathcal{M}^2_{\tilde{\boldsymbol{d}}}$, in the corresponding bases $(\tilde{u}_L, \tilde{c}_L, \tilde{t}_L, \tilde{u}_R, \tilde{c}_R, \tilde{t}_R)$ and $(\tilde{d}_L, \tilde{s}_L, \tilde{b}_L, \tilde{d}_R, \tilde{s}_R, \tilde{b}_R)$. Their complete expressions can be found, e.g., in Ref. [31], and a thorough analysis of the various terms at play can be found in Ref. [29]. Following Ref. [31], we define

$$\mathcal{M}^2_{\tilde{\boldsymbol{d}}} = \begin{pmatrix} M^2_{\tilde{Q}} + m_d^2 + D_{\tilde{d},L} & \frac{v_d}{\sqrt{2}} T_d^\dagger - m_d \mu \tan\beta \\ \frac{v_d}{\sqrt{2}} T_d - m_d \mu^* \tan\beta & M^2_{\tilde{D}} + m_d^2 + D_{\tilde{d},R} \end{pmatrix},$$
$$\mathcal{M}^2_{\tilde{\boldsymbol{u}}} = \begin{pmatrix} V_{\mathrm{CKM}} M^2_{\tilde{Q}} V^\dagger_{\mathrm{CKM}} + m_u^2 + D_{\tilde{u},L} & \frac{v_u}{\sqrt{2}} T_u^\dagger - m_u \frac{\mu}{\tan\beta} \\ \frac{v_u}{\sqrt{2}} T_u - m_u \frac{\mu^*}{\tan\beta} & M^2_{\tilde{U}} + m_u^2 + D_{\tilde{u},R} \end{pmatrix}, \tag{2.11}$$

where $M^2_{\tilde{U}}$, $M^2_{\tilde{D}}$, and $M^2_{\tilde{Q}}$ are the soft breaking squark masses defined in Eq. (2.2), and $m_{u,d}$ are the diagonal up- and down-type quark masses. The various D terms are given by

$$D_{f_{LL,RR}} = \cos 2\beta m_Z^2 (T_f^3 - Q_f \sin^2\theta_W) \mathbb{1}_3, \tag{2.12}$$

which are obviously flavor diagonal.

Finally, the $T_{u,d}$ terms are related to the trilinear quark-squark-Higgs couplings in Eq. (2.4) by

$$(T_u)_{ij} \equiv (A^u Y^u)_{ij}, \tag{2.13}$$

$$(T_d)_{ij} \equiv (A^d Y^d)_{ij}. \tag{2.14}$$

The final mass-ordered squark mass eigenstates are obtained by introducing the unitary transformation to the matrices in Eq. (2.11):

$$\mathrm{diag}(m^2_{\tilde{q}_1}, m^2_{\tilde{q}_2}, \ldots, m^2_{\tilde{q}_6}) = \mathcal{R}_{\tilde{q}} \mathcal{M}^2_{\tilde{q}} \mathcal{R}^\dagger_{\tilde{q}}, \quad \text{for } q = u, d, \quad \text{and} \quad m^2_{\tilde{q}_1} < \ldots < m^2_{\tilde{q}_6}, \tag{2.15}$$

with the matrices $\mathcal{R}_{\tilde{u},\tilde{d}}$ containing the flavor decomposition information of the mass-ordered squark mass eigenstates:

$$(\tilde{u}_1 \ \tilde{u}_2 \ \tilde{u}_3 \ \tilde{u}_4 \ \tilde{u}_5 \ \tilde{u}_6)^t = \mathcal{R}_{\tilde{u}} (\tilde{u}_L \ \tilde{c}_L \ \tilde{t}_L \ \tilde{u}_R \ \tilde{c}_R \ \tilde{t}_R)^t,$$
$$(\tilde{d}_1 \ \tilde{d}_2 \ \tilde{d}_3 \ \tilde{d}_4 \ \tilde{d}_5 \ \tilde{d}_6)^t = \mathcal{R}_{\tilde{d}} (\tilde{d}_L \ \tilde{s}_L \ \tilde{b}_L \ \tilde{d}_R \ \tilde{s}_R \ \tilde{b}_R)^t. \tag{2.16}$$

Transformations between mass and flavor eigenstates are needed to perform phenomenological analyses on the model, as its parameters cannot be accessed directly from the mixed final eigenstates. The complexity of such analyses grows rapidly with the allowed mixings and free parameters. The computational challenge is such that a complete analysis of the most general MSSM with its 105 free parameters is not feasible. We propose two approaches: one within the so-called mass insertion approximation (MIA) with 28 free parameters, and then within a subset of the MSSM including NMFV with 42 parameters.

III. THE MASS INSERTION APPROACH TO THE NMFV MSSM

The usual approach when studying NMFV effects in the MSSM is to use the MIA approach, introduced as early as 1989 in Ref. [32]. The MIA originates as a diagrammatic technique [32,33], allowing us to choose a basis where the quark-squark-neutral gaugino couplings are flavor diagonal. The flavor-changing effects are provided by nondiagonal contributions in the sfermion propagators, as shown in Figs. 1 and 2. The new SUSY contributions (to, e.g., Wilson coefficients) are then proportional to the various off-diagonal elements.

The MIA is also defined algebraically through the flavor expansion theorem (FET) [34], the main features of which

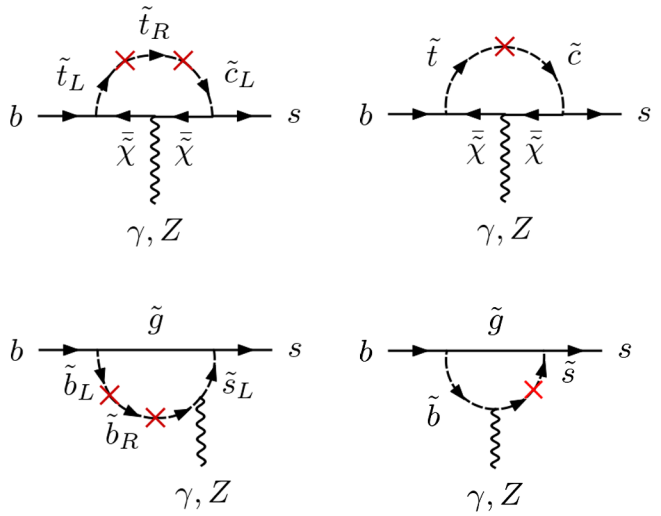

FIG. 1. Some of the relevant penguin diagrams for $b \to s\ell^+\ell^-$. The red cross indicates a Mass Insertion. First row diagrams are based on chargino interactions. The ones at the bottom consider gluino interactions.

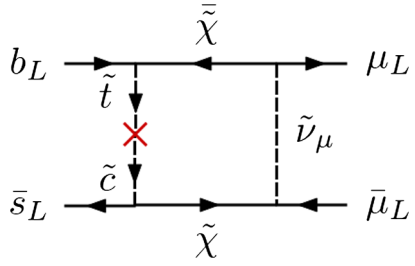

FIG. 2. Relevant box diagram for $b \to s\ell^+\ell^-$. The red cross indicates a Mass Insertion.

we will summarize in the following. All sfermion squared mass matrices M can be decomposed as a sum of a diagonal $\mathrm{diag}(M_{ii}) \equiv M_i^d$ and a nondiagonal $\hat{M}_{ij}$ matrix. Calculating loop amplitudes requires evaluating Hermitian matrix functions $f(M)$ of the involved mass matrices, which can be expanded following the FET's conditions:

$$f(M)_{ij} = \delta_{ij} f(M_i^d) + f^{[1]}(M_i^d, M_j^d)\hat{M}_{ij} + \sum_{n_1} f^{[2]}(M_i^d, M_j^d, M_{n_1}^d)\hat{M}_{in_1}\hat{M}_{jn_1} + \cdots, \quad (3.1)$$

where the divided difference $f^{[k]}$ functions are defined in Ref. [34].

This expansion expresses the loop quantities such as Wilson coefficients in terms of the flavor-violating off-diagonal entries in the squark squared mass matrices. The following dimensionless ratio is usually introduced to define the mass insertions:

$$\delta_{ij}^{\tilde{f}} = \frac{(M_{\tilde{f}}^2)_{ij}}{\sqrt{(M_{\tilde{f}}^2)_{ii}(M_{\tilde{f}}^2)_{jj}}}, \quad (3.2)$$

where $M_{\tilde{f}}^2$ is one of the fermion soft-breaking matrices in Eq. (2.2). As the full sfermion mass matrix is actually a 6×6 matrix spanning both generation and chirality indices [Eq. (2.9)], the actual mass insertion parameter is of the form $(\delta_{ij}^{\tilde{f}})_{AB}$, where i, j are generation indices, and $(AB) \in \{LL, LR, RL, RR\}$.

In this framework, we define the relevant mass insertions (MIs) for our study. To be consistent with the constraints from kaon observables [29,33,35], every off-diagonal element involving a first-generation squark is neglected. The relevant $(\delta_{23}^{\tilde{f}})_{AB}$'s are

$$\delta_{LL}^d = \frac{(M_{\tilde{Q}}^2)_{23}}{(M_{\tilde{Q}})_{22}(M_{\tilde{Q}})_{33}}, \qquad \delta_{RR}^u = \frac{(M_{\tilde{U}}^2)_{23}}{(M_{\tilde{U}})_{22}(M_{\tilde{U}})_{33}}, \qquad \delta_{RR}^d = \frac{(M_{\tilde{D}}^2)_{23}}{(M_{\tilde{D}})_{22}(M_{\tilde{D}})_{33}},$$
$$\delta_{RL}^u = \frac{v_u}{\sqrt{2}}\frac{(T_u)_{23}}{(M_{\tilde{Q}})_{22}(M_{\tilde{U}})_{33}}, \qquad \delta_{LR}^u = \frac{v_u}{\sqrt{2}}\frac{(T_u)_{32}}{(M_{\tilde{Q}})_{33}(M_{\tilde{U}})_{22}},$$
$$\delta_{RL}^d = \frac{v_d}{\sqrt{2}}\frac{(T_d)_{23}}{(M_{\tilde{Q}})_{22}(M_{\tilde{D}})_{33}}, \qquad \delta_{LR}^d = \frac{v_d}{\sqrt{2}}\frac{(T_d)_{32}}{(M_{\tilde{Q}})_{33}(M_{\tilde{D}})_{22}}. \quad (3.3)$$

For the δ_{LL}^u insertion, following the definition of $\mathcal{M}_{\tilde{u}}^2$ in Eq. (2.11), we express it in terms of the soft-breaking squark mass matrix $M_{\tilde{Q}}^2$ as

$$\delta_{LL}^u = \frac{(V_{\mathrm{CKM}} M_{\tilde{Q}}^2 V_{\mathrm{CKM}}^\dagger)_{23}}{(V_{\mathrm{CKM}} M_{\tilde{Q}} V_{\mathrm{CKM}}^\dagger)_{22}(V_{\mathrm{CKM}} M_{\tilde{Q}} V_{\mathrm{CKM}}^\dagger)_{33}}. \quad (3.4)$$

All the relevant NMFV contributions to the C_7, C_9, and C_{10} Wilson coefficients are given in Appendix B.

IV. NUMERICAL SETUP

In what follows, we present a study of NMFV contributions to the $b \to sll$ processes in terms of Wilson coefficients (given in Sec. A 2 of Appendix A) and mass insertions. The model used is an extension of the

TABLE I. SM parameters' values used in this study.

SM parameter	Value
m_t	173.8 GeV
m_b	4.8 GeV
m_c	1.4 GeV
m_s	125 MeV
M_B	5.27 GeV
$\alpha_s(m_Z)$	0.119
$1/\alpha_{el}(m_Z)$	128.9
$\sin^2\theta_W$	0.2334

phenomenological MSSM (pMSSM), where the new contributions arise from additional flavor violation sources in the form of mass insertions. No new sources of CP violation in $\mathcal{L}_{\text{SOFT}}$ with respect to the pMSSM are included, and the degeneracy between the first and second generations of squarks is kept.

The third-generation trilinear interactions A_t, A_b, and A_τ are allowed to vary, while the others are set to zero. As we will see in Sec. VI B 2, the slepton sector contribution to $(g-2)_\mu$ can be completely decoupled from the squark sector analysis. Therefore, no flavor-violating effect is turned on in the slepton sector, as they do not contribute to the $b \to sll$ observables. The Standard Model sector parameters are given in Table I.

The 28 input parameters for our model and their ranges (pMSSM + MIA) are given in Tables II and III. They are randomly sampled from a uniform distribution. The spectrum is calculated at the electroweak scale using the code SOFTSUSY [36]. Following Ref. [30], we have introduced an average squark mass (over the first two generations), obtained from the resulting spectra, and used it to compute the various Wilson coefficients:

$$M_{sq} \equiv \frac{1}{8}\sum_{\text{squarks}} m_{\text{squarks}}. \tag{4.1}$$

We then use SuperIso [37–40] to compute all relevant pMSSM contributions from the obtained spectrum. The

TABLE II. Allowed ranges for the 19 pMSSM soft-breaking parameters.

Parameter	Range
M_1	[50, 5000]
M_2	[50, 5000]
M_3	[50, 5000]
m_A	[50, 5000]
$\tan\beta$	[2, 60]
μ	$[-10^4, 10^4]$
A_t, A_b, A_τ	$[-10^4, 10^4]$
$M_{\tilde{q}_{1L}}, M_{\tilde{q}_{3L}}$	[50, 5000]
$M_{\tilde{u}_R}, M_{\tilde{d}_R}, M_{\tilde{t}_R}, M_{\tilde{b}_R}$	[50, 5000]
$M_{\tilde{e}_L}, M_{\tilde{\tau}_L}, M_{\tilde{e}_R}, M_{\tilde{\tau}_R}$	[50, 5000]

TABLE III. Additional NMFV input parameters in the MIA.

Parameter	Range
$(\delta^{\tilde{u}}_{23})_{LR}$	$[-1, 1]$
$(\delta^{\tilde{u}}_{23})_{LL}$	$[-1, 1]$
$(\delta^{\tilde{u}}_{33})_{LR}$	$[-1, 1]$
$(\delta^{\tilde{d}}_{23})_{LL}$	$[-1, 1]$
$(\delta^{\tilde{d}}_{23})_{RR}$	$[-1, 1]$
$(\delta^{\tilde{d}}_{23})_{RL}$	$[-1, 1]$
$(\delta^{\tilde{d}}_{23})_{LR}$	$[-1, 1]$
$(\delta^{\tilde{d}}_{33})_{RL}$	$[-1, 1]$
$(\delta^{\tilde{d}}_{33})_{LR}$	$[-1, 1]$

additional NMFV contributions to Wilson coefficients are computed following the formulas presented in Appendix B.

A. Constraints

In the following, we give the constraints considered in our study, both during and after the sampling of the parameter space.

First, no tachyonic spectra are kept. This is a built-in condition in many spectrum calculators such as SOFTSUSY, which is enforced during execution.

We discard any spectra with a charged lightest supersymmetric particle (LSP) to ensure the possibility for the LSP (often the lightest neutralino) to be a viable dark matter candidate. We impose further the latest available mass limits from supersymmetric searches given by Ref. [41]. No additional *ab initio* constraints are imposed, in order to keep the study as general as it can be.

As the SLHA1 [42] file format does not implement flavor mixing, the spectrum yielded by SOFTSUSY is obtained without considering the flavor-violating MIA parameters. Therefore, the spectrum considered here is pMSSM-like. The δ's are considered as additional free parameters that do not intervene in the computation of the spectrum. This can be justified *a posteriori* by considering constraints on the MI, as the approximation should be valid if they are small enough with respect to the diagonal mass parameters.

The following limits on the MIA parameters are also considered *a posteriori*:

(1) To avoid tachyonic sparticles, all the MI parameters' ranges are reduced to

$$|\delta^{\tilde{f}}_{AB}| < 0.85. \tag{4.2}$$

(2) From vacuum stability arguments [30,43],

$$|(\delta^{u}_{23})_{LR}| < m_t \frac{\sqrt{2M^2_{sq} + 2\langle m^2_{\tilde{l}}\rangle}}{M^2_{sq}} \simeq \frac{m_t}{M_{sq}}. \tag{4.3}$$

The flavor-violating parameters that contribute the most to C_9 are $(\delta^u_{23})_{LL}$ and $(\delta^u_{23})_{LR}$, in the chargino penguin diagrams such as the ones shown in Fig. 1, which are mainly constrained by Eqs. (4.2) and (4.3). On the other hand, in the $\tilde{d}$ sector, the gluino loops contribute mostly to C_7, which is already strongly limited by experimental data. Therefore, considering all double mass insertions as negligible, no constraints on the other MI parameters are imposed. A comprehensive discussion of the allowed ranges for these parameters can be found in Ref. [44].

Finally, all spectra should be considered with particular care, as flavor mixing can significantly affect the squark masses and their expected signal topologies at colliders. Also, the recast of LHC limits for general MSSM models is a nontrivial task [45,46], which goes beyond the scope of this study. Therefore, no particular limits on the sparticle masses are considered, apart from the model-independent ones present in Ref. [41].

V. RESULTS AND DISCUSSION

The mass insertions allow new sources of FCNC, which give sizeable contributions to flavor observables by significantly shifting the relevant Wilson coefficients. In Fig. 3, we present the scan results with 2×10^6 model points. We can see an oyster-shaped spread of the pMSSM distribution upon turning on the NMFV contributions in the (C_9, C_7) plane. In the (C_9, C_{10}) case, we can see an isotropic spread of the pMSSM distribution in all quadrants, indicating a homogeneous behavior of the two Wilson coefficients under flavor violation in the squark sector. On the other hand, in the (C_9, C_7) case, the largest contribution to C_9 can be obtained by shifting C_7 significantly from its SM value, which is strongly constrained by the $b \to s\gamma$ data. However, it is clear from the impressive spread that the flavor anomalies can be given a satisfying answer using this framework, while still having reasonable values for C_7.

In Fig. 4(a), a zoom in the region of interest in the $(\delta C_9, \delta C_7)$ plane is presented, together with the global best-fit patches from Ref. [47]. δC_i is defined as $C_i^{\mathrm{NMFV}} - C_i^{\mathrm{SM}}$. The pMSSM distribution is shown in red, and the corresponding NMFV points are shown in blue. Imposing the constraints discussed in Sec. IV IV A yields Fig. 4(b) with 1721 remaining points. We can see that even if the highest density of model points can be found away from the C_7 best-fit region, the presented NMFV model succeeds in proposing valid scenarios. In particular, several points seem to completely account for the flavor anomalies in the B sector, but further exploration of the full model spectrum is necessary. Also, it is clear that the pMSSM alone cannot give sufficient contributions to C_9 and C_7: the red distribution can at most account for half of the required shift in C_9 to explain the anomalies, with no other constraints imposed on the pMSSM parameters. Indeed, Fig. 5 clearly shows this feature, where we can see the spread of C_9 for both pMSSM and NMFV models, with no particular constraints on the sampled points. The pMSSM, while being able to provide compelling shifts, fails to fully account for the anomalies (best fit given in Refs. [47–49]) as was shown already in Ref. [22], whereas the NMFV is capable of providing hundreds of compatible scenarios if no other constraints are considered.

To examine these best-fit points, one can look at the associated mass spectra for some well-studied collider SUSY signals like electroweakinos and colored sparticle states. In particular, in Fig. 6, we show both MI parameters and the LSP's mass distribution for our candidate models,

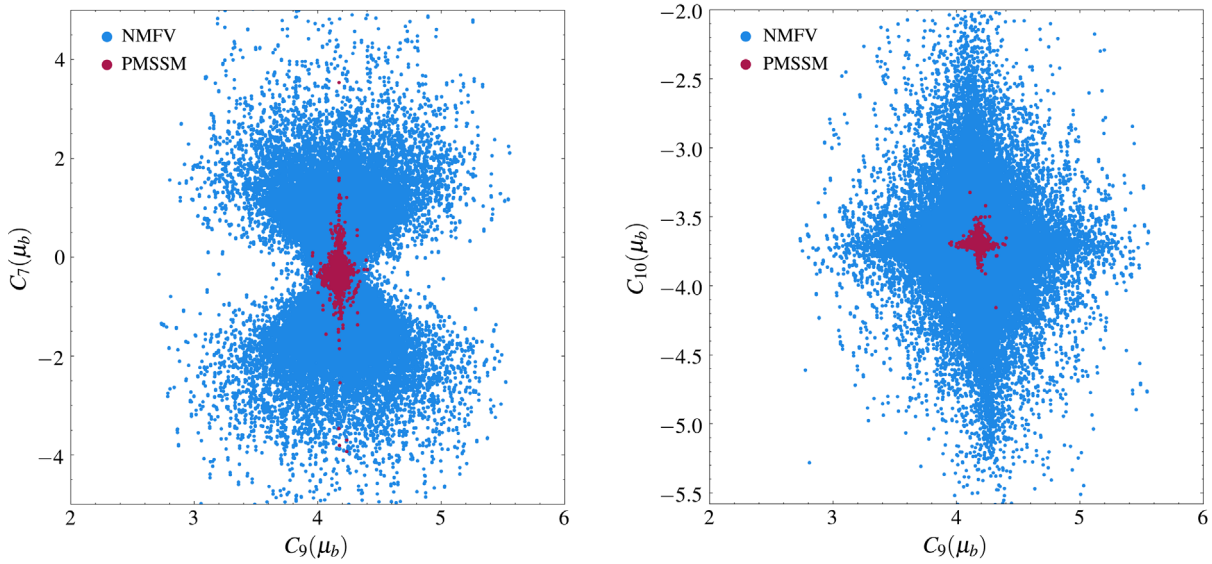

FIG. 3. Combined distributions of the scanned points in the (C_9, C_7) and (C_9, C_{10}) planes. The blue distribution is calculated in the NMFV augmented pMSSM, and the corresponding pMSSM points are shown in red.

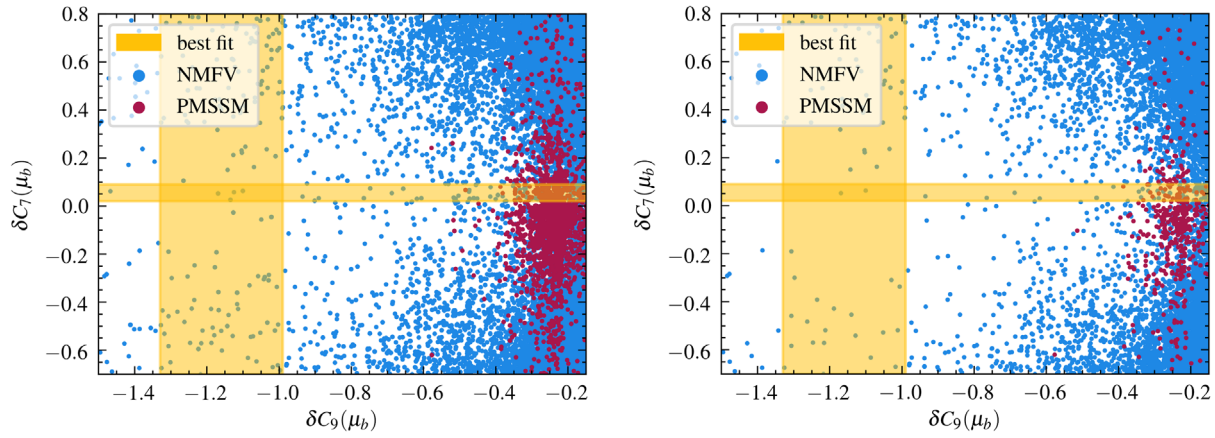

FIG. 4. Combined distribution of the scanned model points in the $(\delta C_9, \delta C_7)$ plane for the whole sample (a) and after applying cuts (b), where $\delta C_i(\mu_b) = C_i^{\mathrm{NMFV,pMSSM}}(\mu_b) - C_i^{\mathrm{SM}}(\mu_b)$. The orange bands represent the 1σ best-fit regions from Ref. [47].

without imposing constraints (left) and after imposing constraints (right) for some of the best points with respect to the expected C_9 shift. We see that a 10% fraction survives the tachyonic and vacuum stability constraints while still offering valid candidates for the flavor anomalies.

Similarly to what was shown in Refs. [30,50], it is mostly the top row diagrams in Fig. 1 corresponding to chargino interactions that contribute the most to C_9, which corresponds to $(\delta^u_{23})_{LR}, (\delta^u_{23})_{LL}$ terms in the MIA. For C_7, the major contributions come from $(\delta^d_{23})_{LR}$ in the gluino diagrams. However, the effect on the Wilson coefficients shown here is the result of a global effect coming from all the contributions. The correlation between the free parameters (pMSSM + MI) and the best (C_9, C_7) values was not found to point towards a specific direction.

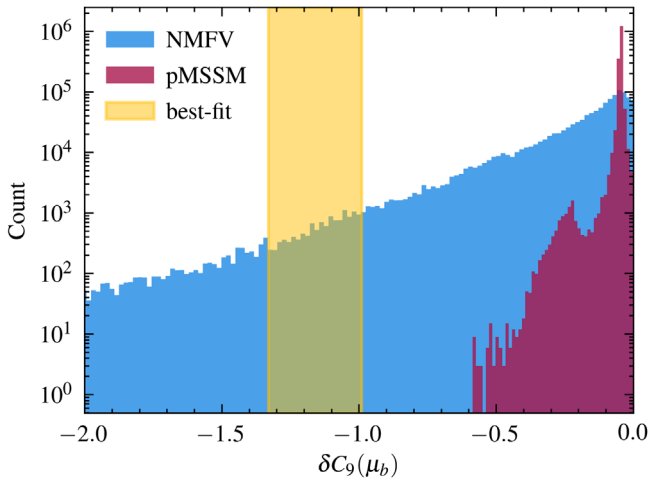

FIG. 5. Compared distribution of $\delta C_9(\mu_b) \leq 0$ for both the pMSSM and our NMFV model. The SM value is shown at the dashed black line, and the best-fit patches are shown in orange. The bins of each histogram differ to show the features of each model.

The effect of the constraints on the most important MI parameters is also shown in Figs. 6(d) and 6(c). From left to right, the available parameter space in the $(\delta_{LL}, \delta^u_{LR})$ plane is reduced from $[-1,1]\times[-1,1]$ to $\simeq[-0.85, 0.85]\times[-0.2, 0.2]$. This shows that vacuum stability constraints on $\tilde{c}_L - \tilde{t}_R$ mixing are the most stringent ones, as expected from large average squark masses, i.e., $M_{sq} \gg 2m_t$. The other MI parameters contribute very little to $C_{7,9}$ and can be neglected and/or kept close to zero.

The results clearly show the interest of NMFV scenarios, and the need of their further exploration. Indeed, the main advantage of the MIA in our case was to easily explore the pMSSM extended with flavor violation, with direct access to the flavor-violating parameters instead of the final mass eigenstates. Also, it has the advantage of reducing the model's free parameters, if their contribution is not significant in the subject at hand, which we did by keeping fewer than 30 parameters, instead of $\mathcal{O}(50)$ or $\mathcal{O}(100)$. However, due to the obviously expected effect on the sparticle spectrum, a more general and complete approach without approximation is necessary to completely confirm the model's shown interesting features. Moreover, a complete approach should also evaluate the contribution of such models to the muon $(g-2)_\mu$. This is precisely what is addressed in the next section.

VI. ANALYTICAL CALCULATIONS IN NMFV-MSSM SCENARIOS WITHOUT APPROXIMATION

In the pMSSM, analytical calculations have been performed for several one-loop quantities such as C_7, C_9 [51], and $(g-2)_\mu$ [52].

In NMFV scenarios, some calculations have been performed at the one-loop level (see, e.g., Refs. [53–55]), but the general contributions to C_7, C_9, and $(g-2)_\mu$ are not

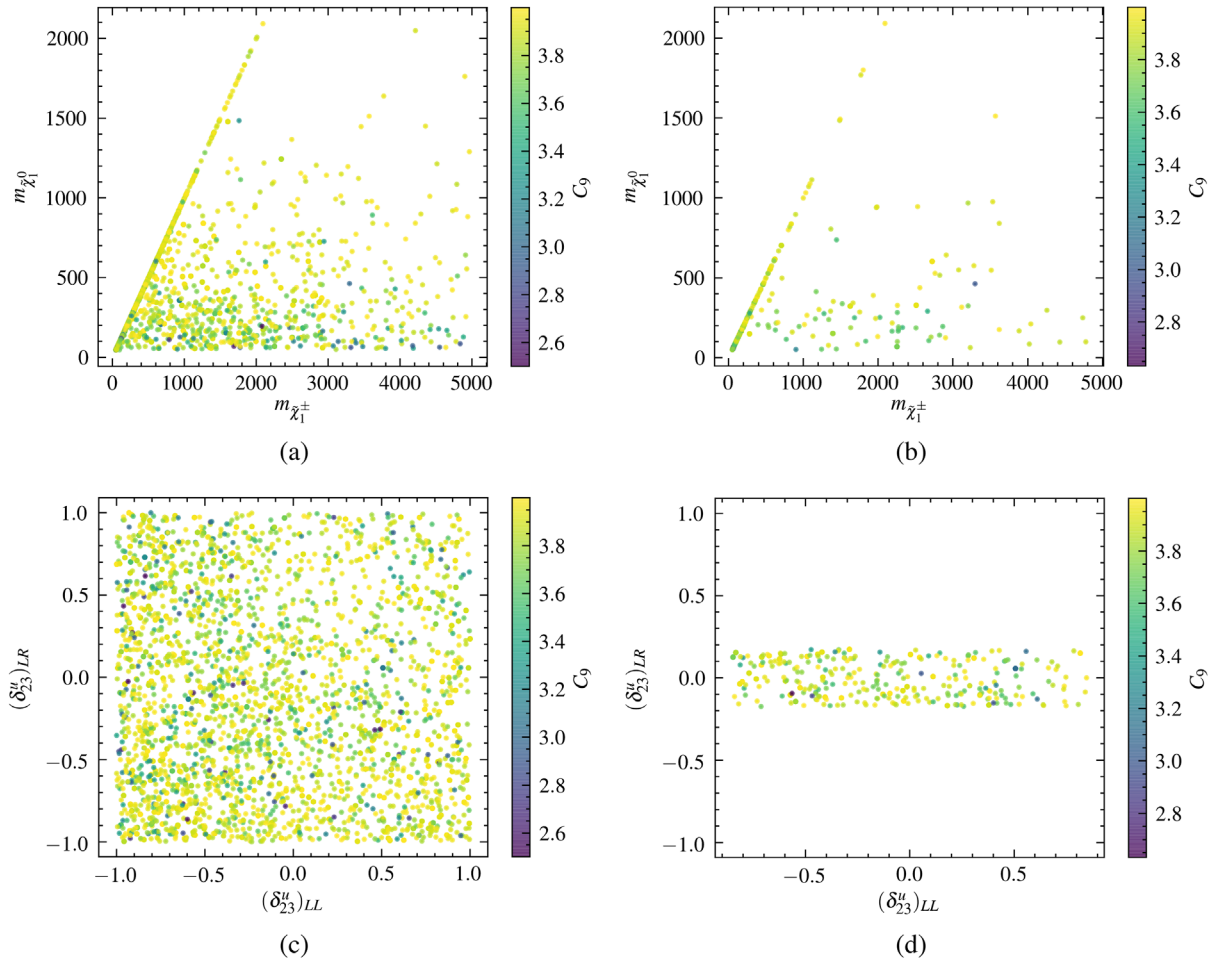

FIG. 6. (a), (b) Distribution of the sampled points in the $(m_{\chi_1^\pm}, m_{\chi_1^0})$ plane, first (top-left) in the case of unconstrained model points that significantly shift the value of C_9. Applying vacuum stability and tachyon constraints on the δ parameters yields the top-right plot. (c), (d) The same goes for the bottom plots, in the $[(\delta_{23}^u)_{LL}, (\delta_{23}^u)_{LR}]$ plane.

known. In the following sections, we present the methods that we used to derive analytically these quantities in the general MSSM with 105 parameters for the first time, together with their evaluation in a particular subset of NMFV scenarios with 42 parameters.

A. Methods

1. Theoretical calculations

In order to derive the full one-loop NMFV contributions to the Wilson coefficients and $(g-2)_\mu$, a large number of Feynman diagrams must be calculated. We performed the analytical calculation in the unconstrained MSSM with general mixings. This means that diagrams must be summed over all particle families: two charginos $\tilde{\chi}^+_{1,2}$, four neutralinos $\tilde{\chi}^0_{1,2,3,4}$, six sleptons $\tilde{l}_{1,2,3,4,5,6}$, six up squarks $\tilde{u}_{1,2,3,4,5,6}$, six down squarks $\tilde{d}_{1,2,3,4,5,6}$, and three sneutrinos $\tilde{\nu}_{1,2,3}$. For the diagram shown in Fig. 7(c), for example, there are $4 \times 4 \times 6 \times 6 \times 2 = 1152$ independent diagrams, where the factor of 2 comes from the two possible contractions for any given ordered pair of neutralinos (counting the crossed diagrams).

We used MARTY [26,27] to calculate automatically all the involved Feynman diagrams and extract the coefficients $(g-2)_\mu$, C_7, and C_9^μ. The number of diagrams for each contribution is presented in Table IV. As MARTY counts left and right Dirac projectors P_L and P_R as independent vertices, the number of diagrams is larger than what a standard counting method would imply.

2. Numerical evaluation

The mathematical expressions resulting from the sum of thousands of one-loop diagrams are too large for any analytical purpose. In order to obtain predictions, MARTY generates a numerical C++ library containing functions evaluating the results given a general MSSM scenario. From a set of values for the SUSY-breaking parameters presented in Eqs. (2.1) to (2.4), we are therefore able to evaluate the exact values of C_7, C_9^μ, and $(g-2)_\mu$ at the one-loop level in the library generated by MARTY.

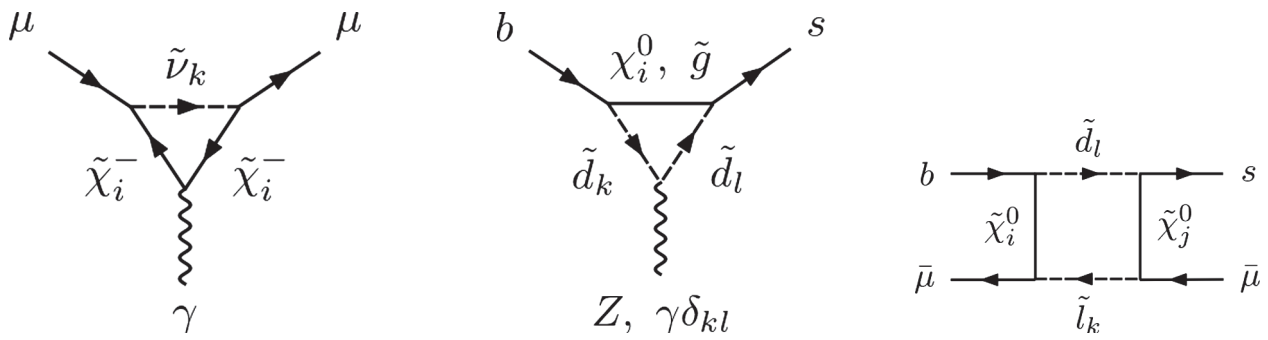

(a) $\tilde{\chi}^+$ penguins in $(g-2)_\mu$ (b) $\tilde{\chi}^0/\tilde{g}$ penguins in C_7 and C_9 (c) $\tilde{\chi}^0$ boxes in C_9^μ

FIG. 7. Examples of contributions in NMFV-MSSM scenarios. Other chargino, neutralino, and Higgs diagrams also contribute to C_7, C_9, and $(g-2)_\mu$.

While MARTY also generates a tree-level spectrum generator to calculate masses and mixings from the initial model parameters, loop corrections are known to be large, and we therefore use SPheno [56,57] to produce a more precise spectrum including loop-level corrections and phenomenological constraints. Finally, the values of the Wilson coefficients are given to SuperIso to apply renormalization group equations and evolve the coefficients down to the b mass scale, and calculate flavor observables.

3. Random scan

To sample the MSSM parameter space, we used a uniform random scan in 42 dimensions with NMFV only in the squark sector to reduce the number of free parameters. Input parameter ranges are presented in Table V.

The scan efficiency is of about 0.05%, corresponding to physical scenarios for which SPheno can calculate a spectrum. For such a low efficiency, there is a large bias in the selected scenarios. Consequently, we also present some posterior distributions of the spectrum in Fig. 8. The scan could be refined with better constraints on the input parameters to improve the efficiency. The following analysis is therefore more a proof of principle rather than a complete phenomenological study of the MSSM parameter space. There are two visible biases in the posterior distributions of spectrum parameters:

(1) Charged sleptons are lighter than sneutrinos because the range for $M^2_{\tilde{E}}$ is smaller than that of $M^2_{\tilde{L}}$.
(2) The lightest neutralino is always lighter than 400 GeV, contrary to the lightest chargino. This is because we impose the condition of having a neutral LSP in order to be a dark matter candidate.

To improve the scan efficiency, we considered machine learning techniques to sample the parameter space. The purpose of these techniques is to create a sampling bias toward scenarios that generate valid model points, that

TABLE IV. Number of diagrams for each contribution calculated by MARTY. The starred numbers are NMFV-specific contributions. By definition, C_7 and $(g-2)_\mu$ only receive contributions from γ-penguin diagrams. There are in total 17949 Feynman diagrams.

	$\tilde{\chi}_i^+$	$\tilde{\chi}_i^0$	$\tilde{g}$	H^+	H^0, A^0
$(g-2)_\mu$	96	96	0	1	2
C_7	240	96*	24*	24	0
C_9/γ penguins	240	96*	24*	24	0
C_9/Z penguins	624	1344*	240*	78	0
C_9/boxes	864	13824*	0	12	0

TABLE V. Input parameters for the scan. Specific ranges have been chosen empirically to improve the scan efficiency. There are in total 42 free parameters, which include the 19 pMSSM parameters and 14 flavor violating parameters $(M^2_{\tilde{Q}})_{23}$, $(M^2_{\tilde{D}})_{23}$, $(A_u)_{ij}$, and $(A_d)_{ij}$ for $i \neq j$.

Parameter	Scanned range
$\tan\beta$	[2, 60]
μ	$[-100, 1000]$ GeV
M_1, M_2	[100, 3000] GeV
M_3	[100, 7000] GeV
M_A	[100, 5000] GeV
$(M^2_{\tilde{Q}})_{ii}$	$[10^2, 10^7]$ GeV^2
$(M^2_{\tilde{U}})_{ii}$	$[10^2, 10^7]$ GeV^2
$(M^2_{\tilde{D}})_{ii}$	$[10^2, 10^7]$ GeV^2
$(M^2_{\tilde{L}})_{ii}$	$[10^2, 10^6]$ GeV^2
$(M^2_{\tilde{E}})_{ii}$	$[10^2, 10^5]$ GeV^2
$(A_e)_{33}$	$[-100, 100]$ GeV
$(A_{u/d})_{11}$	$[-0.1, 0.1]$ GeV
$(A_{u/d})_{22}$	$[-100, 100]$ GeV
$(A_{u/d})_{33}$	$[-10^4, 10^4]$ GeV
$(M^2_{\tilde{Q}})_{23}$	$[0, 10^3]$ GeV^2
$(M^2_{\tilde{D}})_{23}$	$[0, 10^3]$ GeV^2
$(A_u)_{ij}, i \neq j$	$[-100, 100]$ GeV
$(A_d)_{ij}, i \neq j$	$[-100, 100]$ GeV

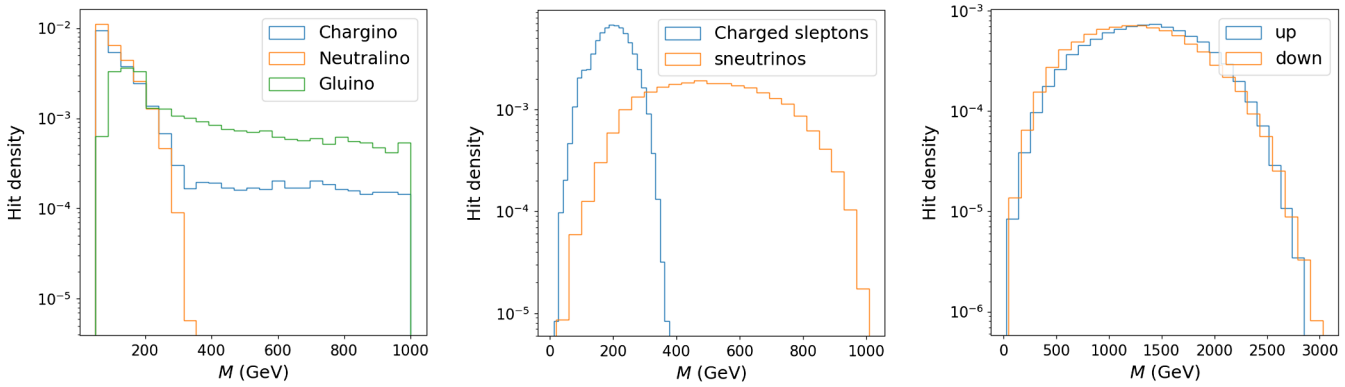

FIG. 8. Posterior distributions for gaugino (left), slepton (middle), and squark (right) masses. For particle families, the distribution corresponds to the lightest particle of the family. Chargino and gluino mass distributions extend up to 3 TeV and 7 TeV, respectively.

therefore improves the scan efficiency. However, while these techniques can be implemented without much difficulty for the pMSSM with 19 parameters, the 43-dimensional space of the NMFV scenarios we present in this paper is too large for the machine-learning-based sampling to be established. Indeed, in the absence of prior knowledge on the distribution of valid parameters, and because of the high number of dimensions, no efficient sampler could be constructed with the considered techniques such as normalizing flows or Hamiltonian Monte Carlo samplers. Further work is required to build efficient samplers in highly dimensional unknown and little-constrained parameter spaces with very few acceptable points, which is beyond the scope of this work.

Finally, let us stress that the current LHC limits on SUSY particle masses are not directly applicable to our study. The NMFV MSSM being a more general model than the so-called simplified or constrained MSSM scenarios, the recasting of collider constraints on the sparticle spectrum is a nontrivial task (see, e.g., Refs. [45,46]) and yields weaker bounds. We nevertheless checked for points leading to significant negative contributions to C_9 that they escape the direct limits, in particular due to the degeneracy between the lightest neutralino and chargino, $\Delta m(\chi_1^0, \chi_1^\pm) \leq 1$ GeV, which makes them extremely complicated to probe experimentally.

B. Results

Using as input the NMFV-MSSM spectra obtained with `SPheno` the numerical functions generated by `MARTY` evaluate the full one-loop contributions to the Wilson coefficients and $(g-2)_\mu$. As the scan is random, we show distributions for the different quantities that we calculated for the 70282 valid model points. In the following, we study the impact on the Wilson coefficients and $(g-2)_\mu$ separately. Then, the relation between the two will be discussed.

1. Wilson coefficients

The distributions for the NMFV-MSSM contributions to the Wilson coefficients C_7 and C_9^μ are presented in Fig. 9.

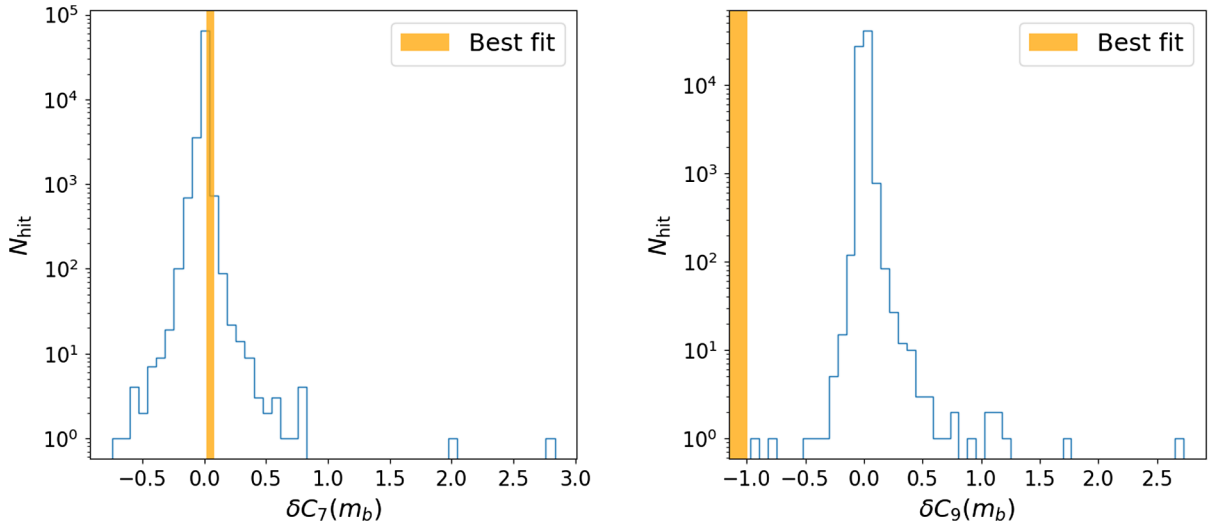

FIG. 9. Distribution of the Wilson coefficients δC_7 and δC_9^μ. The 1σ best-fit regions from Ref. [47] are shown in orange.

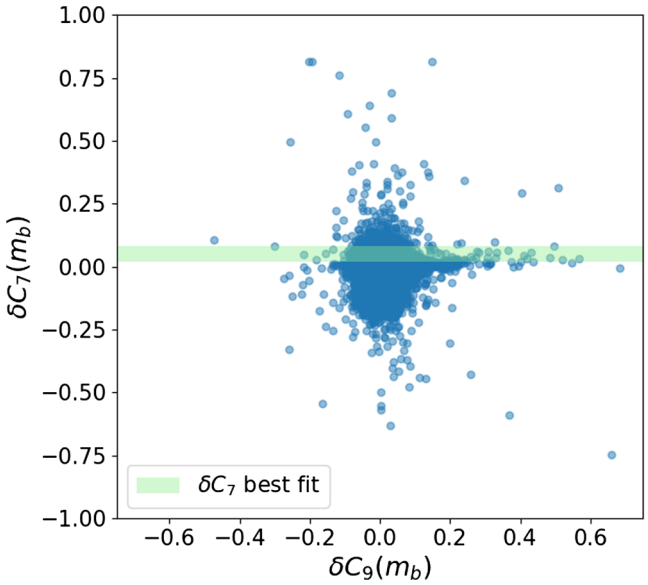

FIG. 10. Combined distribution of the Wilson coefficients δC_7 and δC_9^μ. The best-fit region for δC_7 is shown in green.

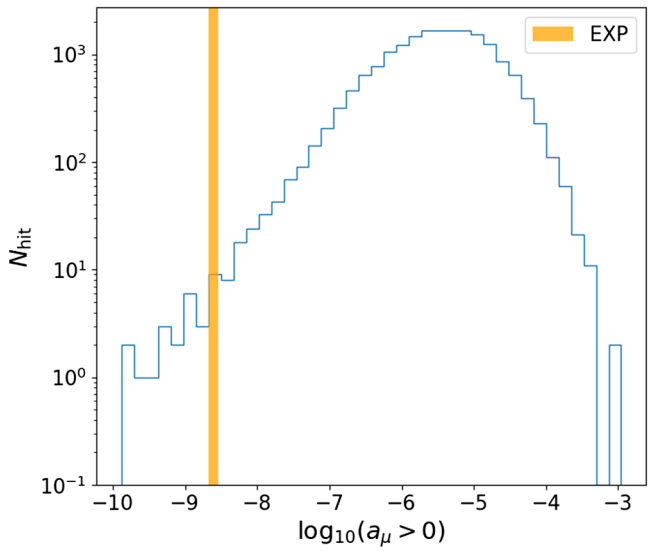

FIG. 11. Distribution of $\delta(g-2)_\mu$. Only scenarios with a positive shift are considered, and the experimental measurement with its 1σ uncertainty [79] is shown in orange.

Both distributions are centered around zero, as expected. While the majority of δC_7 points are close to zero and the best-fit region, many scenarios are already excluded because of a large shift to this coefficient. For δC_9^μ, the best-fit region is shifted by -1 from the SM value. While it is possible to obtain substantial C_9 shifts in our scenarios, only a handful of them predict $\delta C_9^\mu < 0.2$.

It is important to note that the best-fit region for C_9^μ should not be considered as a discriminant criterion; any scenario between the SM and the best fit can still fit better flavor observables and should be carefully considered.

A $2D$ distribution of $(\delta C_7, \delta C_9^\mu)$ is presented in Fig. 10. It is clear that the constraint on δC_7 excludes several scenarios with $\delta C_9^\mu < -0.15$. It seems nevertheless possible to address both coefficients, but a larger dataset is required to explore the region with large negative δC_9.

2. $(g-2)_\mu$ and combined analysis

For just over fifteen years, the anomalous magnetic moment of the muon has proven to be a persistent tension between the SM [58–78] and experimental measurements. The most recent results obtained at Fermilab [79] have not only confirmed the Brookhaven 3σ–4σ [80] discrepancy, but raised it to the 4.2σ level with a combined experimental average of $a_\mu^{\text{EXP}} = 116592061(41) \times 10^{-11}$. However, multiple questions remain, as lattice QCD calculations may reduce the discrepancy to only 1.6σ [81]. In the following, we investigate whether NMFV-MSSM models can account for the observed tensions in both $(g-2)_\mu$ and the b quark flavor sector.

Our present analysis does not strictly consider NMFV parameters in the lepton sector,[1] as shown in Table V. We present the numerical results for $(g-2)_\mu$ in the following. The mass distribution for charged sleptons is around the electroweak scale—i.e., a few hundred GeV (see Fig. 8). This implies significant contributions to $(g-2)_\mu$ that are shown in Fig. 11. As the experimental deviation is very small [79], it is not hard to address $(g-2)_\mu$ alone.

As shown in Table IV, the lepton and quark sectors are sensitive to the neutralino and chargino mass scales. However, while there are slepton contributions in box diagrams for C_9^μ, these contributions are small, and the latter coefficient is almost independent of the slepton masses. Figure 12 shows the dependence of $(g-2)_\mu$ and C_9^μ with respect to the relative slepton mass scale.[2]

This analysis shows that by rescaling the slepton masses (charged sleptons and sneutrinos), one can shift the value of $(g-2)_\mu$ and let Wilson coefficients C_7 and C_9^μ remain stable. It is therefore possible to search for a scenario that fits the flavor observables well and adjust the slepton mass scale to address $(g-2)_\mu$.

VII. CONCLUSION

We presented a first study of the pMSSM extended with nonminimal flavor-violating couplings in the context of the tensions observed in $b \to s\ell^+\ell^-$ transitions with the SM predictions, and we considered the SUSY contributions to

[1]There is no limitation for NMFV in the lepton sector; this choice has been made to reduce the number of free parameters and concentrate on flavor observables that are more difficult to address because of the C_9^μ shift.

[2]C_7 is completely independent of the slepton sector.

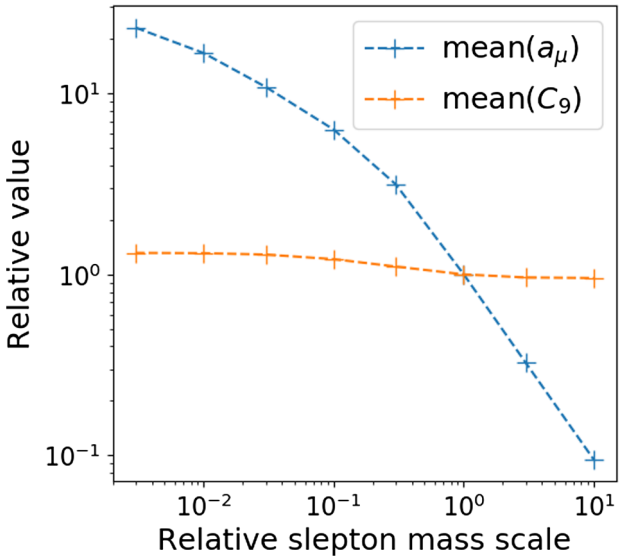

FIG. 12. The variation of the relative mean absolute value of C_9 and $(g-2)_\mu$ for the entire dataset is plotted as a function of the relative slepton mass scale. The initial, nonmodified dataset corresponds to the point at (1,1).

the relevant Wilson coefficients. We carry on our study first by assuming the mass insertion approximation, and then show that the NMFV contributions allow us to shift the Wilson coefficients sufficiently to fully address the anomalies. After imposing theoretical constraints on the flavor-violating parameters, we still find scenarios in agreement with the experimental measurements.

While the MIA provides a direct access to the flavor-violating parameters and eases the phenomenological studies by reducing the number of free parameters, a more general approach is necessary to fully assess the impact of NMFV contributions. Hence, in a second part, we calculated for the first time the full one-loop analytical contributions in the general MSSM to the relevant Wilson coefficients, as well as to $(g-2)_\mu$, using MARTY. By scanning the MSSM parameter space randomly and setting nonzero values for some of the flavor-violating parameters, we obtained 70282 valid scenarios with their individual spectra. In these scenarios, we showed that C_9^μ can be shifted towards the best-fit region given in Ref. [47], but that we have only a few points that shift C_9^μ in the favored direction and let C_7 come close to the SM prediction. We then discussed the scaling of $(g-2)_\mu$ with the slepton mass scale that allows us to address $(g-2)_\mu$ without modifying the predictions for flavor observables.

The present analysis is limited by the small sample of scenarios. For perspective, the scan should be optimized by searching a parameter set that is more likely to produce physical scenarios. In particular, by looking at the posterior distributions of the input parameters, it is possible to refine the scan, improve the efficiency, and generate more scenarios to analyze. Finally, experimental constraints could be studied more in depth to compare the obtained spectra with direct searches of SUSY particles, in particular from LHC measurements. The obtained results are nevertheless very promising and show for the first time the impact of NMFV parameters in addressing the recent anomalies.

ACKNOWLEDGMENTS

We would like to thank Gérald Grenier, Sabine Kraml, Gaël Alguero, Björn Herrmann, and Abdelhamid Boussejra for helpful discussions and insights.

APPENDIX A: WILSON COEFFICIENTS

1. Effective Hamiltonian at the electroweak scale

The effective Hamiltonian for the decay $B \to X_s \ell^+ \ell^-$ in the SM and in the MSSM is given by (neglecting the small contribution proportional to $V_{us}^* V_{ub}$), in the basis of Ref. [30],

$$\mathcal{H}_{\text{eff}} = -\frac{4G_F}{\sqrt{2}} V_{ts}^* V_{tb} \left[\sum_{i=1}^{8} C_i(\mu) O_i + \frac{\alpha}{4\pi} \sum_{i=9}^{10} \tilde{C}_i(\mu) O_i \right], \tag{A1}$$

where the O_i operators read

$$\begin{aligned}
O_1 &= \bar{s}_{L\alpha} \gamma_\mu b_{L\alpha} \bar{c}_{L\beta} \gamma^\mu c_{L\beta}, \\
O_2 &= \bar{s}_{L\alpha} \gamma_\mu b_{L\beta} \bar{c}_{L\beta} \gamma^\mu c_{L\alpha}, \\
O_3 &= \bar{s}_{L\alpha} \gamma_\mu b_{L\alpha} \sum_{q=u,\ldots,b} \bar{q}_{L\beta} \gamma^\mu q_{L\beta}, \\
O_4 &= \bar{s}_{L\alpha} \gamma_\mu b_{L\beta} \sum_{q=u,\ldots,b} \bar{q}_{L\beta} \gamma^\mu q_{L\alpha}, \\
O_5 &= \bar{s}_{L\alpha} \gamma_\mu b_{L\alpha} \sum_{q=u,\ldots,b} \bar{q}_{R\beta} \gamma^\mu q_{R\beta}, \\
O_6 &= \bar{s}_{L\alpha} \gamma_\mu b_{L\beta} \sum_{q=u,\ldots,b} \bar{q}_{R\beta} \gamma^\mu q_{R\alpha}, \\
O_7 &= \frac{e}{16\pi^2} m_b \bar{s}_L \sigma^{\mu\nu} b_R F_{\mu\nu}, \\
O_8 &= \frac{g_s}{16\pi^2} m_b \bar{s}_L T^a \sigma^{\mu\nu} b_R G^a_{\mu\nu}, \\
O_9 &= (\bar{s}_L \gamma_\mu b_L) \bar{l} \gamma^\mu l, \\
O_{10} &= (\bar{s}_L \gamma_\mu b_L) \bar{l} \gamma^\mu \gamma_5 l,
\end{aligned}$$

with V being the CKM matrix and $q_{L(R)} = \frac{(1 \mp \gamma_5)}{2} q$.

This Hamiltonian is known to next-to-leading order both in the SM [82,83] and in the MSSM [84–86].

For the B system, the operators and coefficients of interest for the anomalies are C_7, C_9, and C_{10}.

2. Wilson coefficients

We consider the contributions to the Wilson coefficients as given in Ref. [30], including the correction as suggested

in Ref. [50], which we reproduce here for completeness. The loop functions $P_{ijk}(a,b)$ are defined in Appendix B. The constants are as follows:

(1) θ_W is the weak mixing angle of the SM for the electroweak bosons.
(2) M_W^2 is the squared mass of the $W^\pm$ boson.
(3) $\lambda_{t,b}$ are the Yukawa couplings for the top and bottom quarks.
(4) g_2 is the weak isospin coupling constant.
(5) M_{sq} is the average squark mass.
(6) $M_{\tilde{g}}$ is the gluino mass.
(7) In $P_{ijk}(x_i,x_j)$, x_i, and x_j are defined as $M_{\tilde{\chi}_i}^2/M_{sq}^2$ for chargino loops.
(8) In $P_{ijk}(x,x)$, x is defined as $M_{\tilde{g}}^2/M_{sq}^2$, for gluino graphs.
(9) The V_{ab}'s are the elements of the CKM matrix.
(10) $m_{s,b}$ are the pole masses of the s, b quarks.
(11) $N_c = 3$ is the number of color charges in $SU(3)_c$.
(12) α_s is the QCD coupling constant, evaluated at M_Z.
(13) G_F is the Fermi constant.
(14) U, V are the charginos mixing matrices defined in eq. (A2).

In the weak eigenstates basis, the chargino mass matrix is given by [29]

$$M_\chi = \begin{pmatrix} M_2 & \sqrt{2}M_W \sin\beta \\ \sqrt{2}M_W \cos\beta & \mu \end{pmatrix}, \tag{A2}$$

where the index 1 of rows and columns refers to the wino, and the index 2 to the Higgsino. μ is the Higgs quadratic coupling, and M_2 is the soft SUSY-breaking wino mass. The 3×3 complex matrices U and V which diagonalize M_χ are introduced:

$$\mathrm{diag}(M_{\chi_1}, M_{\chi_2}) = U^* M_\chi V^+. \tag{A3}$$

Their explicit expressions can be found in, e.g., Ref. [87]. All the contributions to the Wilson coefficients are evaluated at the renormalization scale $\mu_0 = m_W$.

a. Chargino contributions

In the following, we give the contributions from chargino loops, such as the two top diagrams in Fig. 1.

Z-penguin with Higgsino/wino loops:

$$-\frac{C_9}{1-4\sin^2\theta_W} = C_{10} = (\delta_{23}^u)_{LR}\frac{\lambda_t}{g_2}\frac{V_{cs}^*}{V_{ts}^*}\frac{1}{4\sin^2\theta_W}\sum_{i,j=1,2} V_{i1}V_{j2}^* \times\left\{U_{i1}^* U_{j1}\sqrt{x_i x_j}P_{112}(x_i,x_j) + V_{i1}^* V_{j1} P_{111}(x_i,x_j) - \frac{1}{2}\delta_{ij}P_{021}(x_i,x_j)\right\}. \tag{A4}$$

This diagram is proportional to $(\delta_{23}^u)_{LR}$, which is one of the most interesting mass insertions, and is yet to be more constrained.

Z-penguin with two wino vertices:

$$-\frac{C_9}{1-4\sin^2\theta_W} = C_{10} = -(\delta_{23}^u)_{LL}\frac{V_{cs}^*}{V_{ts}^*}\frac{1}{4\sin^2\theta_W}\sum_{i,j=1,2} V_{i1}V_{j1}^* \times\{U_{i1}^* U_{j1}\sqrt{x_i x_j}P_{112}(x_i,x_j) + V_{i1}^* V_{j1} P_{111}(x_i,x_j) - \delta_{ij}P_{021}(x_i,x_j)\}. \tag{A5}$$

This is the same diagram as above, but with the exchange of two winos. They differ only by the specific mass insertion and the factor λ_t/g_2. Both diagrams are null in the limit of a diagonal chargino mass matrix, and so they are negligible for large M_2.

Gamma penguin with two wino vertices:

$$C_7 = -(\delta_{23}^u)_{LL}\frac{M_W^2}{M_{sq}^2}\frac{1}{3}\frac{V_{cs}^*}{V_{ts}^*}\sum_{i=1,2} V_{i1}V_{i1}^*\left\{\frac{3}{2}P_{222}(x_i,x_i) + P_{132}(x_i,x_i)\right\}, \tag{A6}$$

$$C_9 = -(\delta_{23}^u)_{LL}\frac{M_W^2}{M_{sq}^2}\frac{2}{3}\frac{V_{cs}^*}{V_{ts}^*}\times\sum_{i=1,2} V_{i1}V_{i1}^*\left\{P_{312}(x_i,x_i) - \frac{1}{3}P_{042}(x_i,x_i) + x_i P_{313}(x_i,x_i)\right\}, \tag{A7}$$

$$C_7' = -(\delta_{23}^u)_{LL}\frac{M_W^2}{M_{sq}^2}\frac{1}{3}\frac{V_{cs}^*}{V_{ts}^*}\frac{m_s}{m_b}\sum_{i=1,2} V_{i1}V_{i1}^*\left\{\frac{3}{2}P_{222}(x_i,x_i) + P_{132}(x_i,x_i)\right\}. \tag{A8}$$

Gamma penguin with Higgsino-wino vertex:

$$C_7 = \frac{M_W^2}{M_{sq}^2}\frac{V_{cs}^*}{V_{ts}^*}\sum_{i=1,2}\left[V_{i2}^* V_{i1}\frac{\lambda_t}{g_2}\left\{\frac{1}{2}P_{222}(x_i,x_i)+\frac{1}{3}P_{132}(x_i,x_i)\right\}(\delta_{23}^u)_{LR}\right.$$
$$\left. + U_{i2}V_{i1}\frac{M_{\chi_i}}{m_b}\frac{\lambda_b}{g_2}\left\{P_{212}(x_i,x_i)+\frac{2}{3}P_{122}(x_i,x_i)\right\}(\delta_{23}^u)_{LL}\right], \tag{A9}$$

$$C_9 = (\delta_{23}^u)_{LR}\frac{M_W^2}{M_{sq}^2}\frac{2}{3}\frac{\lambda_t}{g_2}\frac{V_{cs}^*}{V_{ts}^*}\sum_{i=1,2}V_{i2}^*V_{i1}\left\{P_{312}(x_i,x_i)-\frac{1}{3}P_{042}(x_i,x_i)+x_iP_{313}(x_i,x_i)\right\}, \tag{A10}$$

$$C_7' = (\delta_{23}^u)_{LR}\frac{M_W^2}{M_{sq}^2}\frac{1}{3}\frac{\lambda_t}{g_2}\frac{V_{cs}^*}{V_{ts}^*}\frac{m_s}{m_b}\sum_{i=1,2}V_{i2}^*V_{i1}\left\{\frac{3}{2}P_{222}(x_i,x_i)+P_{132}(x_i,x_i)\right\}. \tag{A11}$$

The primed operators are obtained by switching the chirality of external states. All of these contributions are used, but we are most interested in the C_9 contribution coming from the $\gamma\tilde{H}\tilde{W}$ vertex.

Z-penguin with two wino vertices and a double mass insertion:

Even though a double mass insertion corresponds to a higher order in the perturbative expansion, it has been pointed out [30] that this particular diagram could provide enhancement in the K system. For completeness, in the B decay, the contribution is

$$-\frac{C_9}{1-4\sin^2\theta_W} = C_{10} = -\frac{(\delta_{23}^u)_{LR}(\delta_{33}^u)_{LR}}{4\sin^2\theta_W}\frac{V_{cs}^*}{V_{ts}^*}\sum_{i,j=1,2}V_{i1}V_{j1}^*$$
$$\times\left\{U_{i1}^*U_{j1}\sqrt{x_ix_j}P_{123}(x_i,x_j)+\frac{1}{2}V_{i1}^*V_{j1}P_{122}(x_i,x_j)-\frac{\delta_{ij}}{3}P_{032}(x_i,x_j)\right\}. \tag{A12}$$

b. Gluino contribution

In this part, we collect all the contributions arising from gluino loops, from the bottom diagrams in Fig. 1, with $x \equiv M_{\tilde{g}}^2/M_{sq}^2$.

γ-penguin:

$$C_7 = \frac{\sqrt{2}}{M_{sq}^2G_F}\frac{1}{3}\frac{N_c^2-1}{2N_c}\frac{\pi\alpha_s}{V_{ts}^*V_{tb}}\left[\left((\delta_{23}^d)_{LL}+(\delta_{23}^d)_{RR}\frac{m_s}{m_b}\right)\frac{1}{4}P_{132}(x,x)+(\delta_{23}^d)_{RL}P_{122}(x,x)\frac{M_{\tilde{g}}}{m_b}\right], \tag{A13}$$

$$C_7' = \frac{\sqrt{2}}{M_{sq}^2G_F}\frac{1}{3}\frac{N_c^2-1}{2N_c}\frac{\pi\alpha_s}{V_{ts}^*V_{tb}}\left[\left((\delta_{23}^d)_{RR}+(\delta_{23}^d)_{LL}\frac{m_s}{m_b}\right)\frac{1}{4}P_{132}(x,x)+(\delta_{23}^d)_{LR}P_{122}(x,x)\frac{M_{\tilde{g}}}{m_b}\right], \tag{A14}$$

$$C_9 = -\frac{\sqrt{2}}{M_{sq}^2G_F}\frac{1}{3}\frac{N_c^2-1}{2N_c}\frac{\pi\alpha_s}{V_{ts}^*V_{tb}}\frac{1}{3}P_{042}(x,x)(\delta_{23}^d)_{LL}, \tag{A15}$$

$$C_9' = -\frac{\sqrt{2}}{M_{sq}^2G_F}\frac{1}{3}\frac{N_c^2-1}{2N_c}\frac{\pi\alpha_s}{V_{ts}^*V_{tb}}\frac{1}{3}P_{042}(x,x)(\delta_{23}^d)_{RR}. \tag{A16}$$

The terms proportional to $M_{\tilde{g}}$ can be dominant over the others. However, the mass insertion which enters the diagram is strongly constrained from $b \to s\gamma$ [32].

Double mass insertion, $Z-\tilde{g}$:

For completeness, we give the gluino penguin contribution with a double mass insertion:

$$-\frac{C_9}{1-4\sin^2\theta_W} = C_{10} = \frac{(\delta_{33}^d)_{LR}(\delta_{23}^d)_{RL}}{V_{tb}V_{ts}^*}\frac{N_c^2-1}{2N_c}\frac{\alpha_s}{12\alpha}P_{032}(x,x), \tag{A17}$$

$$-\frac{C_9'}{1-4\sin^2\theta_W} = C_{10}' = \frac{(\delta_{33}^d)_{RL}(\delta_{23}^d)_{LR}}{V_{tb}V_{ts}^*}\frac{N_c^2-1}{2N_c}\frac{\alpha_s}{12\alpha}P_{122}(x,x). \tag{A18}$$

c. Box diagrams

The following contributions come from the box diagrams in Fig 2.

Box diagram with wino exchange:

$$C_9 = -C_{10} = (\delta_{23}^u)_{LL}\frac{V_{cs}^*}{V_{ts}^*}\frac{M_W^2}{M_{sq}^2}\frac{1}{\sin^2\theta_W}\sum_{i,j=1,2}(V_{i1}^*V_{j1}V_{i1}V_{j1}^*)f(x_i,x_j,x_{\tilde{\nu}}), \tag{A19}$$

where

$$f(x_i,x_j,x_{\tilde{\nu}}) = \frac{1}{2}\int_0^1 dx\int_0^1 dy\int_0^1 dz\frac{yz(1-z)^2}{[y(1-z)+x_{\tilde{\nu}}(1-y)(1-z)+z(x_ix+x_j(1-x))]^2} \tag{A20}$$

and $x_{\tilde{\nu}} = M_{\tilde{\nu}}^2/M_{sq}^2$.

Box diagram with Higgsino-bottom-stop vertex:
Replacing the wino with a Higgsino yields

$$C_9 = -C_{10} = -(\delta_{23}^u)_{LR}\frac{V_{cs}^*}{V_{ts}^*}\frac{M_W^2}{M_{sq}^2}\frac{\lambda_t}{g_2\sin^2\theta_W}\sum_{i,j=1,2}(V_{i1}^*V_{j1}V_{i1}V_{j2}^*)f(x_i,x_j,x_{\tilde{\nu}}). \tag{A21}$$

APPENDIX B: FEYNMAN INTEGRALS AND HYPER-GEOMETRIC FUNCTIONS

1. Hypergeometric functions and integral representations

To calculate the new Wilson coefficients in the NMFV/MIA framework, the following integrals need to be evaluated:

$$P_{ijk}(a,b) \equiv \int_0^1 dx\int_0^1 dy\frac{y^i(1-y)^j}{(1-y+axy+b(1-x)y)^k}. \tag{B1}$$

These integrals can be shown to be linear combinations of hypergeometric functions ${}_pF_q$ (for an extensive review see Refs. [88,89]). In most cases, the integrals can be rewritten using solely ${}_2F_1$, which is sometimes referred to as the Gaussian or ordinary hypergeometric function. This leads to nearly arbitrary precision in the numerical implementation as the series usually converge quickly. However, in some cases, particular analytical continuation formulas have to be used, which are well known in the literature, and can be found in, e.g., Ref. [88].

The integral representation of ${}_2F_1$ is defined by Euler's formula:

$${}_2F_1(a,b;c;z) = \frac{\Gamma(c)}{\Gamma(b)\Gamma(c-b)}\times\int_0^1 t^{b-1}(1-t)^{c-b-1}(1-tz)^{-a}\mathrm{d}t, \tag{B2}$$

which is a one-valued analytic function of z, provided $\Re(c) > \Re(b) > 0, |\arg(1-z)| < \pi$ [88].

In what follows, we will refer to ${}_2F_1$ as simply F. Equation (B2) provides an analytic continuation of F, which is usually defined by its series representation:

$$F(a,b;c;z) \coloneqq \sum_{n=0}^{\infty}\frac{(a)_n(b)_n}{(c)_n}\frac{z^n}{n!}, \tag{B3}$$

where

$(a)_n = \dfrac{\Gamma(a+n)}{\Gamma(a)}$, is the (rising) Pochhammer symbol.

The generalized hypergeometric functions ${}_pF_q$ can be defined by

$${}_pF_q\left(\begin{bmatrix}a_1,\ldots,a_p\\ b_1,\ldots,b_q\end{bmatrix};z\right) = \sum_{n=0}^{\infty}\frac{(a_1)_n\cdots(a_p)_n}{(b_1)_n\cdots(b_q)_n}\frac{z^n}{n!}, \tag{B4}$$

and a general Euler integral transform relates hypergeometric functions of higher and lower orders [89]:

$$ {}_{A+1}F_{B+1}\left[\begin{matrix} a_1,\ldots,a_A,c \\ b_1,\ldots,b_B,d \end{matrix};z\right] = \frac{\Gamma(d)}{\Gamma(c)\Gamma(d-c)}\int_0^1 t^{c-1}(1-t)^{d-c-1}\,{}_AF_B\left[\begin{matrix} a_1,\ldots,a_A \\ b_1,\ldots,b_B \end{matrix};tz\right]. \tag{B5} $$

2. Analytical expressions for P_{ijk}

Let us demonstrate that the class of loop integrals in Eq. (B1) can all be expressed using hypergeometric functions.

First, we rewrite Eq. (B1) using Fubini's theorem as

$$ P_{ijk}(a,b) = \int_0^1 \mathrm{d}y\, y^i(1-y)^j \int_0^1 \mathrm{d}x \frac{1}{[A(a,b;y)x + B(b;y)]^k}, \tag{B6} $$

with

$$ A(a,b;y) = y(a-b), \tag{B7} $$

$$ B(b;y) = 1 + y(b-1). \tag{B8} $$

Therefore, for $\mathbf{k} \neq \mathbf{1}$ and $\mathbf{a} \neq \mathbf{b}$, we can integrate over x using Cavalieri's quadrature formula:

$$ \int_0^1 \frac{\mathrm{d}x}{(B+Ax)^k} = \left[\frac{(Ax+B)^{1-k}}{(1-k)A}\right]_0^1 = \frac{(A+B)^{1-k} - B^{1-k}}{A(1-k)}. \tag{B9} $$

Then, by replacing the integrand in Eq. (B6) with the result of Eq. (B9), we obtain

$$ P_{ijk}(a,b) = \int_0^1 \mathrm{d}y \frac{y^{i-1}(1-y)^j}{(a-b)(1-k)}[(y(a-1)+1)^{1-k} - (y(b-1)+1)^{1-k}]. \tag{B10} $$

We can spot the integral representation of the hypergeometric function. Explicitly,

$$ \begin{aligned} P_{ijk}(a,b) &= \frac{1}{a-b}\frac{1}{1-k}\int_0^1 \mathrm{d}y\, y^{i-1}(1-y)^j[(1-y(1-a))^{1-k} - a \leftrightarrow b] \\ &= \frac{\beta_E(i,j+1)}{(a-b)(1-k)}[F(k-1,i;i+j+1;1-a) - a \leftrightarrow b], \end{aligned} \tag{B11} $$

where we use Eq. (B2) and Euler's beta function's definition.

$k \neq 1$, $a = b$:

Let $G(b) = F(k-1,i;i+j+1;1-b)$. By definition,

$$ \lim_{a\to b}\frac{G(a)-G(b)}{a-b} = G'(b), \tag{B12} $$

and the differentiation formula for F is

$$ \frac{\mathrm{d}F(\alpha,\beta;\gamma;z)}{\mathrm{d}z} = \frac{\alpha\beta}{\gamma}F(\alpha+1,\beta+1;\gamma+1;z). \tag{B13} $$

Therefore,

$$ \lim_{a\to b}P_{ijk}(a,b) = \beta_E(i,j+1)\lim_{a\to b}\frac{1}{(1-k)(a-b)}[G(a)-G(b)], \tag{B14} $$

$$ = \frac{\beta_E(i,j+1)}{1-k}G'(b), \tag{B15} $$

$$ = \frac{1}{1-k}\beta_E(i,j+1)\frac{(k-1)i}{(i+j+1)}F(k,i+1;i+j+2;1-b), \tag{B16} $$

which simplifies to

$$ P_{ijk}(b,b) = \beta_E(i+1,j+1)F(k,i+1,i+j+2;1-b). \tag{B17} $$

$k = 1$:

Only three of these integrals appear in the computation of the Wilson coefficients; all three are reasonably doable:

$$ P_{111}(a,b) = \int_{[0,1]^2}\mathrm{d}x\mathrm{d}y\frac{y(1-y)}{1-y+axy+b(1-x)y}, \tag{B18} $$

$$ P_{021}(a,a) = \int_{[0,1]^2}\mathrm{d}x\mathrm{d}y\frac{(1-y)^2}{1+y(a-1)}, \tag{B19} $$

$$ P_{111}(a,a) = \int_{[0,1]^2}\mathrm{d}x\mathrm{d}y\frac{y(1-y)}{1+y(a-1)}. \tag{B20} $$

The last two integrals are straightforward to compute:

$$
\begin{aligned}
P_{111}(a,a) &= \int_0^1 \mathrm{d}y \frac{y(1-y)}{1+y(a-1)}, \\
&= \frac{1}{a-1}\left([y(y-1)\log(1+y(a-1))]_0^1 - \int_0^1 (1-2y)\log((1+y(a-1))\mathrm{d}y\right), \\
&= \frac{-1}{a-1}\int_0^1 \mathrm{d}y(1-2y)\log((1+y(a-1)), \\
&= \frac{-1}{a-1}\frac{-a^2+2a\log(a)+1}{2(a-1)^2},
\end{aligned} \tag{B21}
$$

with

$$
\lim_{a\to 1}\frac{-1}{a-1}\frac{-a^2+2a\log(a)+1}{2(a-1)^2} = \frac{1}{6}.
$$

Similarly,

$$
\begin{aligned}
P_{021}(a,a) &= \int_{[0,1]^2} \mathrm{d}x\mathrm{d}y \frac{(1-y)^2}{1+y(a-1)} = \frac{-1}{a-1}\int_0^1 \mathrm{d}y 2(1-y)\log\left(1+y(a-1)\right), \\
&= \frac{(a+1)(3a^2-2a^2\log(a)-4a+1)}{2(a-1)^2 a},
\end{aligned} \tag{B22}
$$

with

$$
\lim_{a\to 1}\frac{(a+1)(3a^2-2a^2\log(a)-4a+1)}{2(a-1)^2 a} = 0,
$$

$$
P_{111}(a,b) = \int_{[0,1]^2} \mathrm{d}x\mathrm{d}y \frac{y(1-y)}{1-y+axy+b(1-x)y}, \tag{B23}
$$

$$
\begin{aligned}
&= \frac{1}{2(a-1)^2(a-b)(b-1)^2(ab-a-b+1)} \\
&\times \Bigg[(a-1)^2(a-b)(b-1)^2 + (a-1)^2(b-1)^2\log\left(\frac{a}{b}\right)(ab-a-b+1) \\
&+ (a-1)^2(2b-1)(-\log b)(ab-a-b+1) \\
&+ (2a-1)(b-1)^2\log(a)(ab-a-b+1)\Bigg].
\end{aligned} \tag{B24}
$$

For completeness, let us show that in this case too, we can reexpress $P_{ij1}(a,b)$ using hypergeometric functions:

We are interested in the set of integrals defined by

$$
P_{ij1}(a,b) = \int_0^1 \mathrm{d}x \int_0^1 \mathrm{d}y \frac{y^i(1-y)^j}{1-y+axy+b(1-x)y}. \tag{B25}
$$

Two cases, $a = b$ and $a \neq b$, have to be distinguished.

$k = 1$, $a = b$:

In this case, the computation is straightforward and yields

$$
\begin{aligned}
P_{ij1}(a,b) &= \int_0^1 \mathrm{d}x \int_0^1 \mathrm{d}y \frac{y^i(1-y)^j}{1-y+axy+b(1-x)y} \\
&= \int_0^1 \mathrm{d}y \frac{y^i(1-y)^j}{(1-y(1-a))}
\end{aligned} \tag{B26}
$$

$$
= \beta_E(i+1,j+1)\,{}_2F_1(1,i+1;i+j+2;1-a). \tag{B27}
$$

$k = 1$, $a \neq b$:

We can express Eq. (B25) as an integral over ${}_2F_1$:

$$P_{ij1}(a,b) = \int_0^1 \mathrm{d}x \int_0^1 \mathrm{d}y \frac{y^i(1-y)^j}{1-y+axy+b(1-x)y}$$
$$= \int_0^1 \mathrm{d}x \int_0^1 \mathrm{d}y y^i(1-y)^j(1-y(1-b-x(a-b))) \tag{B28}$$
$$= \int_0^1 \mathrm{d}x \beta_E(i+1,j+1)\,{}_2F_1(1,i+1;i+j+2;1-b-x(a-b)). \tag{B29}$$

This holds provided $\mathrm{Re}\{1-ax-b(1-x)\} < 1$. For $x \in [0,1]$, $a,b \in \mathcal{R}^+$, this is always true.

Using the general Euler transform [Eq. (B5)], we can compute the integral over ${}_2F_1$:

$$P_{ij1}(a,b) = \beta_E(i+1,j+1)\frac{1}{a-b}\left((1-a)\,{}_3F_2\left[\begin{matrix}1,1,i+1\\2,i+j+2\end{matrix};1-a\right] - a \leftrightarrow b\right). \tag{B30}$$

The two previous results for $a = b$ and $a \neq b$ can be checked against the explicit analytical expressions given before.

[1] LHCb Collaboration, Measurement of Form-Factor-Independent Observables in the Decay $B^0 \to K^{*0}\mu^+\mu^-$, Phys. Rev. Lett. **111**, 191801 (2013).

[2] LHCb Collaboration, Differential branching fractions and isospin asymmetries of $B \to K^{(*)}\mu^+\mu^-$ decays, J. High Energy Phys. 06 (2014) 133.

[3] LHCb Collaboration, Differential branching fraction and angular analysis of $\Lambda_b^0 \to \Lambda\mu^+\mu^-$ decays, J. High Energy Phys. 06 (2015) 115.

[4] LHCb Collaboration, Angular Analysis of the $B^+ \to K^{*+}\mu^+\mu^-$ Decay, Phys. Rev. Lett. **126**, 161802 (2021).

[5] LHCb Collaboration, Branching Fraction Measurements of the Rare $B_s^0 \to \phi\mu^+\mu^-$ and $B_s^0 \to f_2'(1525)\mu^+\mu^-$ Decays, Phys. Rev. Lett. **127**, 151801 (2021).

[6] LHCb Collaboration, Test of lepton universality with $B^0 \to K^{*0}\ell^+\ell^-$ decays, J. High Energy Phys. 08 (2017) 055.

[7] LHCb Collaboration, Test of lepton universality in beauty-quark decays, Nat. Phys. **18**, 277 (2022).

[8] S. Descotes-Genon, J. Matias, and J. Virto, Understanding the $B \to K^*\mu^+\mu^-$ Anomaly, Phys. Rev. D **88**, 074002 (2013).

[9] W. Altmannshofer and D. M. Straub, New physics in $B \to K^*\mu\mu$?, Eur. Phys. J. C **73**, 2646 (2013).

[10] T. Hurth and F. Mahmoudi, On the LHCb anomaly in $B \to K^*\ell^+\ell^-$, J. High Energy Phys. 04 (2014) 097.

[11] T. Hurth, F. Mahmoudi, and S. Neshatpour, Global fits to $b \to s\ell\ell$ data and signs for lepton non-universality, J. High Energy Phys. 12 (2014) 053.

[12] T. Hurth, F. Mahmoudi, and S. Neshatpour, On the anomalies in the latest LHCb data, Nucl. Phys. **B909**, 737 (2016).

[13] J. Wess and B. Zumino, Supergauge transformations in four dimensions, Nucl. Phys. **B70**, 39 (1974).

[14] P. Fayet, Supersymmetry and weak, electromagnetic and strong interactions, Phys. Lett. **64B**, 159 (1976).

[15] H. P. Nilles, Supersymmetry, supergravity and particle physics, Phys. Rep. **110**, 1 (1984).

[16] MSSM Working Group Collaboration, The minimal supersymmetric standard model: Group summary report, in GDR (Groupement De Recherche)—Supersymetrie, 12, 1998 [arXiv:hep-ph/9901246].

[17] C. F. Berger, J. S. Gainer, J. L. Hewett, and T. G. Rizzo, Supersymmetry without prejudice, J. High Energy Phys. 02 (2009) 023.

[18] S. S. AbdusSalam, B. C. Allanach, F. Quevedo, F. Feroz, and M. Hobson, Fitting the phenomenological MSSM, Phys. Rev. D **81**, 095012 (2010).

[19] S. Sekmen, S. Kraml, J. Lykken, F. Moortgat, S. Padhi, L. Pape, M. Pierini, H. B. Prosper, and M. Spiropulu, Interpreting LHC SUSY searches in the phenomenological MSSM, J. High Energy Phys. 02 (2012) 075.

[20] A. Arbey, M. Battaglia, and F. Mahmoudi, Implications of LHC searches on SUSY particle spectra: The pMSSM parameter space with neutralino dark matter, Eur. Phys. J. C **72**, 1847 (2012).

[21] A. Arbey, M. Battaglia, and F. Mahmoudi, Constraints on the MSSM from the Higgs sector: A pMSSM study of Higgs searches, $B_s^0 \to \mu^+\mu^-$ and dark matter direct detection, Eur. Phys. J. C **72**, 1906 (2012).

[22] F. Mahmoudi, S. Neshatpour, and J. Virto, $B \to K^*\mu^+\mu^-$ optimised observables in the MSSM, Eur. Phys. J. C **74**, 2927 (2014).

[23] Q.-Y. Hu, Y.-D. Yang, and M.-D. Zheng, Revisiting the B-physics anomalies in R-parity violating MSSM, Eur. Phys. J. C **80**, 365 (2020).

[24] P. S. Bhupal Dev, A. Soni, and F. Xu, Hints of natural supersymmetry in flavor anomalies? arXiv:2106.15647.

[25] M. A. Boussejra and F. Mahmoudi, New constraints on flavour violating supersymmetry, Proc. Sci., EPS-HEP2021 (**2022**) 661.

[26] G. Uhlrich, F. Mahmoudi, and A. Arbey, MARTY—Modern ARtificial Theoretical phYsicist A C++ framework automating symbolic calculations beyond the standard model, Comput. Phys. Commun. **264**, 107928 (2021).

[27] G. Uhlrich, F. Mahmoudi, and A. Arbey, Automatic extraction of one-loop Wilson coefficients in general BSM scenarios using MARTY-1.4, Proc. Sci., EPS-HEP2021 (**2022**) 507.

[28] S. P. Martin, A supersymmetry primer, Adv. Ser. Dir. High Energy Phys. **18**, 1 (1998).

[29] M. Drees, R. Godbole, and P. Roy, Theory and Phenomenology of Sparticles: An Account of Four-Dimensional $N = 1$ Supersymmetry in High Energy Physics (World Scientific, Singapore, 2005).

[30] E. Lunghi, A. Masiero, I. Scimemi, and L. Silvestrini, B → $X_s\ell^+\ell^-$ decays in supersymmetry, Nucl. Phys. **B568**, 120 (2000).

[31] B. C. Allanach *et al.*, SUSY Les Houches Accord 2, Comput. Phys. Commun. **180**, 8 (2009).

[32] F. Gabbiani and A. Masiero, FCNC in generalized supersymmetric theories, Nucl. Phys. **B322**, 235 (1989).

[33] E. Gabrielli, A. Masiero, and L. Silvestrini, Flavor changing neutral currents and *CP* violating processes in generalized supersymmetric theories, Phys. Lett. B **374**, 80 (1996).

[34] A. Dedes, M. Paraskevas, J. Rosiek, K. Suxho, and K. Tamvakis, Mass insertions vs. mass eigenstates calculations in flavour physics, J. High Energy Phys. 06 (2015) 151.

[35] M. Ciuchini, A. Masiero, P. Paradisi, L. Silvestrini, S. K. Vempati, and O. Vives, Soft SUSY breaking grand unification: Leptons versus quarks on the flavor playground, Nucl. Phys. **B783**, 112 (2007).

[36] B. C. Allanach, SOFTSUSY: A program for calculating supersymmetric spectra, Comput. Phys. Commun. **143**, 305 (2002).

[37] F. Mahmoudi, SuperIso: A program for calculating the isospin asymmetry of $B \to K^*\gamma$ gamma in the MSSM, Comput. Phys. Commun. **178**, 745 (2008).

[38] F. Mahmoudi, SuperIso v2.3: A program for calculating flavor physics observables in supersymmetry, Comput. Phys. Commun. **180**, 1579 (2009).

[39] F. Mahmoudi, SuperIso v3.0, flavor physics observables calculations: Extension to NMSSM, Comput. Phys. Commun. **180**, 1718 (2009).

[40] S. Neshatpour and F. Mahmoudi, Flavour Physics with SuperIso, Proc. Sci., TOOLS2020 (**2021**) 036.

[41] Particle Data Group, Review of Particle Physics, Prog. Theor. Exp. Phys. **2020**, 083C01 (2020).

[42] P. Z. Skands *et al.*, SUSY Les Houches accord: Interfacing SUSY spectrum calculators, decay packages, and event generators, J. High Energy Phys. 07 (2004) 036.

[43] J. A. Casas and S. Dimopoulos, Stability bounds on flavor violating trilinear soft terms in the MSSM, Phys. Lett. B **387**, 107 (1996).

[44] K. De Causmaecker, B. Fuks, B. Herrmann, F. Mahmoudi, B. O'Leary, W. Porod, S. Sekmen, and N. Strobbe, General squark flavour mixing: Constraints, phenomenology and benchmarks, J. High Energy Phys. 11 (2015) 125.

[45] J. Bernigaud and B. Herrmann, First steps towards the reconstruction of the squark flavour structure, SciPost Phys. **6**, 066 (2019).

[46] G. Alguero, J. Heisig, C. Khosa, S. Kraml, S. Kulkarni, A. Lessa *et al.*, Constraining new physics with SModelS version 2, arXiv:2112.00769.

[47] T. Hurth, F. Mahmoudi, D. M. Santos, and S. Neshatpour, More indications for lepton nonuniversality in $b \to s\ell^+\ell^-$, Phys. Lett. B **824**, 136838 (2022).

[48] T. Hurth, F. Mahmoudi, D. Martinez Santos, and S. Neshatpour, Lepton nonuniversality in exclusive $b \to s\ell\ell$ decays, Phys. Rev. D **96**, 095034 (2017).

[49] A. Arbey, T. Hurth, F. Mahmoudi, D. M. Santos, and S. Neshatpour, Update on the b → s anomalies, Phys. Rev. D **100**, 015045 (2019).

[50] A. Behring, C. Gross, G. Hiller, and S. Schacht, Squark flavor implications from $\bar{B} \to \bar{k}^* l^+ l^-$, J. High Energy Phys. 08 (2012) 152.

[51] C. Bobeth, A. J. Buras, and T. Ewerth, $\bar{B} \to X_s\ell^+\ell^-$ in the MSSM at NNLO, Nucl. Phys. **B713**, 522 (2005).

[52] S. P. Martin and J. D. Wells, Muon anomalous magnetic dipole moment in supersymmetric theories, Phys. Rev. D **64**, 035003 (2001).

[53] A. Dedes, J. Rosiek, and P. Tanedo, Complete one-loop MSSM predictions for $B_0 \to \ell^+\ell^-$ at the Tevatron and LHC, Phys. Rev. D **79**, 055006 (2009).

[54] A. Crivellin, L. Hofer, and J. Rosiek, Complete resummation of chirally-enhanced loop-effects in the MSSM with non-minimal sources of flavor-violation, J. High Energy Phys. 07 (2011) 017.

[55] A. Crivellin and U. Nierste, Chirally enhanced corrections to flavor-changing neutral current processes in the generic MSSM, Phys. Rev. D **81**, 095007 (2010).

[56] W. Porod, SPheno, a program for calculating supersymmetric spectra, SUSY particle decays and SUSY particle production at e^+e^- colliders, Comput. Phys. Commun. **153**, 275 (2003).

[57] W. Porod and F. Staub, SPheno 3.1: Extensions including flavour, *CP*-phases and models beyond the MSSM, Comput. Phys. Commun. **183**, 2458 (2012).

[58] T. Aoyama *et al.*, The anomalous magnetic moment of the muon in the Standard Model, Phys. Rep. **887**, 1 (2020).

[59] T. Aoyama, M. Hayakawa, T. Kinoshita, and M. Nio, Complete Tenth-Order QED Contribution to the Muon $g-2$, Phys. Rev. Lett. **109**, 111808 (2012).

[60] T. Aoyama, T. Kinoshita, and M. Nio, Theory of the anomalous magnetic moment of the electron, Atoms **7**, 28 (2019).

[61] A. Czarnecki, W. J. Marciano, and A. Vainshtein, Refinements in electroweak contributions to the muon anomalous magnetic moment, Phys. Rev. D **67**, 073006 (2003).

[62] C. Gnendiger, D. Stöckinger, and H. Stöckinger-Kim, The electroweak contributions to $(g-2)_\mu$ after the Higgs boson mass measurement, Phys. Rev. D **88**, 053005 (2013).

[63] M. Davier, A. Hoecker, B. Malaescu, and Z. Zhang, Reevaluation of the hadronic vacuum polarisation contributions to the Standard Model predictions of the muon $g-2$

and $\alpha(m_Z^2)$ using newest hadronic cross-section data, Eur. Phys. J. C **77**, 827 (2017).
[64] A. Keshavarzi, D. Nomura, and T. Teubner, Muon $g-2$ and $\alpha(M_Z^2)$: A new data-based analysis, Phys. Rev. D **97**, 114025 (2018).
[65] G. Colangelo, M. Hoferichter, and P. Stoffer, Two-pion contribution to hadronic vacuum polarization, J. High Energy Phys. 02 (2019) 006.
[66] M. Hoferichter, B.-L. Hoid, and B. Kubis, Three-pion contribution to hadronic vacuum polarization, J. High Energy Phys. 08 (2019) 137.
[67] M. Davier, A. Hoecker, B. Malaescu, and Z. Zhang, A new evaluation of the hadronic vacuum polarisation contributions to the muon anomalous magnetic moment and to $\boldsymbol{\alpha(m_Z^2)}$, Eur. Phys. J. C **80**, 241 (2020).
[68] A. Keshavarzi, D. Nomura, and T. Teubner, The $g-2$ of charged leptons, $\alpha(M_Z^2)$ and the hyperfine splitting of muonium, Phys. Rev. D **101**, 014029 (2020).
[69] A. Kurz, T. Liu, P. Marquard, and M. Steinhauser, Hadronic contribution to the muon anomalous magnetic moment to next-to-next-to-leading order, Phys. Lett. B **734**, 144 (2014).
[70] K. Melnikov and A. Vainshtein, Hadronic light-by-light scattering contribution to the muon anomalous magnetic moment revisited, Phys. Rev. D **70**, 113006 (2004).
[71] P. Masjuan and P. Sánchez-Puertas, Pseudoscalar-pole contribution to the $(g_\mu-2)$: A rational approach, Phys. Rev. D **95**, 054026 (2017).
[72] G. Colangelo, M. Hoferichter, M. Procura, and P. Stoffer, Dispersion relation for hadronic light-by-light scattering: Two-pion contributions, J. High Energy Phys. 04 (2017) 161.
[73] M. Hoferichter, B.-L. Hoid, B. Kubis, S. Leupold, and S. P. Schneider, Dispersion relation for hadronic light-by-light scattering: Pion pole, J. High Energy Phys. 10 (2018) 141.
[74] A. Gérardin, H. B. Meyer, and A. Nyffeler, Lattice calculation of the pion transition form factor with $N_f = 2+1$ Wilson quarks, Phys. Rev. D **100**, 034520 (2019).
[75] J. Bijnens, N. Hermansson-Truedsson, and A. Rodríguez-Sánchez, Short-distance constraints for the HLbL contribution to the muon anomalous magnetic moment, Phys. Lett. B **798**, 134994 (2019).
[76] G. Colangelo, F. Hagelstein, M. Hoferichter, L. Laub, and P. Stoffer, Longitudinal short-distance constraints for the hadronic light-by-light contribution to $(g-2)_\mu$ with large-N_c Regge models, J. High Energy Phys. 03 (2020) 101.
[77] T. Blum, N. Christ, M. Hayakawa, T. Izubuchi, L. Jin, C. Jung, and C. Lehner, The Hadronic Light-by-Light Scattering Contribution to the Muon Anomalous Magnetic Moment from Lattice QCD, Phys. Rev. Lett. **124**, 132002 (2020).
[78] G. Colangelo, M. Hoferichter, A. Nyffeler, M. Passera, and P. Stoffer, Remarks on higher-order hadronic corrections to the muon $g-2$, Phys. Lett. B **735**, 90 (2014).
[79] Muon $g-2$ Collaboration, Measurement of the Positive Muon Anomalous Magnetic Moment to 0.46 ppm, Phys. Rev. Lett. **126**, 141801 (2021).
[80] Muon $g-2$ Collaboration, Final report of the muon E821 anomalous magnetic moment measurement at BNL, Phys. Rev. D **73**, 072003 (2006).
[81] S. Borsanyi *et al.*, Leading hadronic contribution to the muon magnetic moment from lattice QCD, Nature (London) **593**, 51 (2021).
[82] A. J. Buras and M. Munz, Effective Hamiltonian for $B \to X_s e^+ e^-$ beyond leading logarithms in the NDR and HV schemes, Phys. Rev. D **52**, 186 (1995).
[83] G. Buchalla, A. J. Buras, and M. E. Lautenbacher, Weak decays beyond leading logarithms, Rev. Mod. Phys. **68**, 1125 (1996).
[84] P. L. Cho, M. Misiak, and D. Wyler, $K_L \to \pi^0 e^+ e^-$ and $B \to X_s \ell^+ \ell^-$ decay in the MSSM, Phys. Rev. D **54**, 3329 (1996).
[85] T. Goto, Y. Okada, Y. Shimizu, and M. Tanaka, $b \to \mathrm{sl}\,\bar{l}$ in the minimal supergravity model, Phys. Rev. D **55**, 4273 (1997).
[86] T. Goto, Y. Okada, and Y. Shimizu, Flavor changing neutral current processes in B and K decays in the supergravity model, Phys. Rev. D **58**, 094006 (1998).
[87] F. Kruger and J. Romao, Flavor conserving CP phases in supersymmetry and implications for exclusive B decays, Phys. Rev. D **62**, 034020 (2000).
[88] H. Bateman, *Higher Transcendental Functions [Vol. I–III]* (McGraw-Hill Book Company, New York, 1953), Vol. 1.
[89] L. Slater, *Generalized Hypergeometric Functions* (Cambridge University Press, Cambridge, England, 2008).